International Journal of Solids and Structures 306 (2025) 113103

Contents lists available at ScienceDirect

International Journal of Solids and Structures

journal homepage: www.elsevier.com/locate/ijsolstr

Elastic wave propagation in periodic stress-driven nonlocal Timoshenko beams

Gioacchino Alotta *, Andrea Francesco Russillo, Giuseppe Failla

Department of Civil, Energy, Environmental and Materials Engineering (DICEAM), University of Reggio Calabria, via Zehender, 89124 Reggio Calabria, Italy

ARTICLE INFO

Keywords:
Small-size beam
Stress-driven nonlocal elasticity theory
Elastic wave propagation
Periodicity
Local resonance

ABSTRACT

Nonlocal theories are well established to model statics and dynamics of small-size structures. Recent studies investigated elastic wave propagation in nonlocal beams and attention focused on periodic nonlocal beams, either endowed with resonators or resting on supports, for relevant applications at small scale. In this context, this work proposes a stress-driven nonlocal Timoshenko beam formulation and develops an original and comprehensive analytical/computational framework for wave propagation analysis in bare and periodic beams.

The framework addresses infinite and finite beams. First, exact analytical expressions are derived for the dispersion curves of the bare beam, which provide full insight into the effects of nonlocality. Second, an exact Plane Wave Expansion method is devised for periodic beams, either equipped with mass-spring resonators or resting on elastic supports; both $\omega(q)$ and $q(\omega)$ dispersion curves are derived in this work, where ω is the frequency and q is the wave number. Third, an approximate homogenization approach is formulated to estimate opening frequencies and sizes of band gaps induced by mass-spring resonators. Finally, a two-field finite element method is proposed to calculate the transmittance of finite periodic beams.

Numerical applications investigate the dispersion diagram of bare and periodic beams for different internal lengths of the stress-driven nonlocal model. Remarkably, results for finite periodic beams validate the predictions from wave propagation analysis of corresponding infinite ones. Moreover, parametric analyses show the capability of the stress-driven nonlocal model in capturing typical small-size effects.

1. Introduction

Statics and dynamics of small-size structures are subjects of great importance in modern mechanics, in view of the many applications of this type of structures in micro- and nano-engineering (Thai et al., 2017; Roudbari et al., 2022; Ghavanloo et al., 2023). Since the early stages of research in this field, considerable effort was devoted to developing theoretical and computational models capable, on one hand, of capturing size effects not predicted by the classical free-scale continuum approach and implementable, on the other hand, at relatively low computational costs compared to the very demanding atomistic simulations. This is the research framework where nonlocal or generalized continuum theories were formulated, as Eringen's nonlocal integral theory and its differential counterpart (Eringen, 1972, 1983; Numanoğlu et al., 2018; Numanoğlu and Civalek, 2019; Zhang et al., 2020; Zhao et al., 2021), strain gradient theories (Aifantis, 1999, 2003, 2009, 2011; Askes and Aifantis, 2011; Challamel et al., 2016; Polizzotto, 2014, 2015; Akgöz and Civalek, 2014), nonlocal strain gradient theories (Lim et al., 2015; Zhang and Qing, 2021b; Bian and Qing, 2021), nonlocal stress gradient theories (Li and Qing, 2024; Zhang and Qing, 2023), micropolar "Cosserat" theory (Lakes, 1991), couple stress theory (Mindlin, 1963; Yang et al., 2002), peridynamic theory (Silling, 2000; Silling et al., 2007), mechanically-based approaches involving long-range interactions among non-adjacent volumes (Di Paola et al., 2009, 2010, 2013; Failla et al., 2010; Alotta et al., 2014, 2017, 2018), fractional-calculus based theories (Patnaik and Semperlotti, 2020; Patnaik et al., 2020, 2021; Alotta et al., 2022). More recently, the new stress-driven nonlocal theory (Romano and Barretta, 2017a,b; Romano et al., 2017a) gained popularity as effective formulation to study small-size structures, with applications to beams/frames (Romano and Barretta, 2017a,b; Romano et al., 2017a; Barretta et al., 2018; Russillo et al., 2021; Caporale et al., 2023; Behnam-Rasouli et al., 2024) and 3D solids (Russillo et al., 2022). Its fundamental assumption is that the strain at a material point depends on the stresses at different material points via a convolution integral with space-dependent attenuation function; from the integral formulation, an equivalent differential formulation can be derived, on assuming the attenuation function in exponential form. The stress-driven nonlocal theory proved well posed in statics (Romano and Barretta, 2017b;

* Corresponding author.
E-mail address: gioacchino.alotta@unirc.it (G. Alotta).

https://doi.org/10.1016/j.ijsolstr.2024.113103
Received 14 June 2024; Received in revised form 26 September 2024; Accepted 8 October 2024
Available online 10 October 2024

Zhang and Qing, 2021a; Qing and Tang, 2023; Scorza et al., 2022; Tang and Qing, 2024), in dynamics (He et al., 2020; Russillo et al., 2021; Zhang and Qing, 2022a; Zhang et al., 2022a,b; Zhang and Qing, 2022b) and capable of overcoming some paradoxes derived from the Eringen's nonlocal differential theory for specific problems involving the statics of beams (Romano et al., 2017b), targeted as benchmark problems and solved by alternative strategies as well (see Demir and Civalek (2017) and references therein). Comprehensive reviews on nonlocal and generalized continua may be found in Thai et al. (2017), Roudbari et al. (2022), Ghavanloo et al. (2023).

Modelling elastic wave propagation in small-size structures is a relevant application field of nonlocal or generalized continuum theories, as demonstrated by an increasing number of studies in the last few years. Indeed, many works focused on wave propagation in small-size beams (Wang and Hu, 2005; Lu et al., 2007; Lim et al., 2015; De Domenico and Askes, 2018; Askes and Aifantis, 2009; Gomez-Silva and Askes, 2024), adopting the Eringen's nonlocal differential theory (Wang and Hu, 2005; Lu et al., 2007), stress gradient or combined strain/inertia gradient theories (Askes and Aifantis, 2009), a higher-order nonlocal strain gradient theory of elasticity built upon the Eringen's nonlocal integral theory (Lim et al., 2015), a three-length-scale gradient theory (De Domenico and Askes, 2018), a variationally consistent formulation with long-range forces (Gomez-Silva and Askes, 2024). The Euler-Bernoulli beam model was used in Wang and Hu (2005), Lu et al. (2007), Lim et al. (2015), Askes and Aifantis (2009), De Domenico and Askes (2018), the Timoshenko beam model in Wang and Hu (2005), Lim et al. (2015), Askes and Aifantis (2009), De Domenico and Askes (2018), an Elishakoff beam model derived from the Timoshenko one in Gomez-Silva and Askes (2024). Very recently, the stress-driven nonlocal theory in conjunction with the Euler-Bernoulli beam model was adopted in Barretta et al. (2024) to investigate wave propagation in nanobeams, either bare or resting on nano-foundations. Other works addressed functionally-graded nanobeams, using a nonlocal strain gradient theory (Ebrahimi et al., 2019) or the so-called general nonlocal theory (Faroughi et al., 2020) developed in Shaat (2017) via a suitable modification of the Eringen's nonlocal integral theory; in these cases, a refined higher-order beam model (Ebrahimi et al., 2019) and the Reddy's beam model (Faroughi et al., 2020) were used. Interesting reviews on the studies dealing with wave propagation in small-size beams can be found in Thai et al. (2017), Roudbari et al. (2022), Farajpour et al. (2018), Eltaher et al. (2016).

Dealing with wave propagation in small-size beams, several studies addressed not only bare beams but also periodic ones, with periodicity due to alternate materials, equally spaced supports or resonant attachments (Chen and Wang, 2011; Allegri et al., 2013; Yan et al., 2020; Deng et al., 2017a,b; Trabelssi et al., 2024; Zhou et al., 2019; Qian, 2020; Qian et al., 2021; Qian and Wang, 2022; Espo et al., 2022). These beams are of particular interest because their frequency response may exhibit band gaps, i.e., frequency ranges where waves do not propagate, with obvious benefits in terms of vibration reduction. Longitudinal wave propagation in small-size beams made of two alternate materials, modelling phononic crystals, was investigated in Chen and Wang (2011) and in Yan et al. (2020) using the Eringen's nonlocal differential theory. Moreover, flexural wave propagation in small-size beams on periodically spaced supports was studied in Allegri et al. (2013), Deng et al. (2017a,b), using the Eringen's nonlocal differential theory (Allegri et al., 2013; Deng et al., 2017b) or the modified couple stress theory (Deng et al., 2017a) in conjunction with the Euler-Bernoulli beam model; in particular, these studies focused on multi-span graphene nanoribbons (Allegri et al., 2013) and multi-span functionally graded nanopipes (Deng et al., 2017b) or micropipes conveying fluid (Deng et al., 2017a). Very recently, flexural wave propagation in small-size beams with periodically spaced mass-spring resonant attachments was studied in Trabelssi et al. (2024), based on the nonlocal strain gradient theory. The work in Trabelssi et al. (2024) can be cast within the emerging research area on *metamaterial* nanobeams; other examples in this respect are the work in Zhou et al. (2019) on the size-dependent flexural wave band gap formation in phononic crystal nanobeams with surface effects, as well as the works in Qian (2020), Qian et al. (2021) on piezoelectric phononic crystal nanobeams (Qian et al., 2021) and piezoelectric phononic crystal nanobeams with periodically spaced "mass-spring" resonators (Qian, 2020); they used the Timoshenko beam model (Qian et al., 2021) and the Euler-Bernoulli beam model (Qian, 2020), including surface elasticity in both cases. Moreover, building on the models used in Qian (2020), Qian et al. (2021), a new type of resonator was devised in Qian and Wang (2022) to control the electromechanical coupling bandgap of phonic crystal nanobeams equipped with periodically spaced horizontal and vertical resonators. Another study in this field was conducted in Espo et al. (2022) on piezoelectric phononic crystal nanobeams, using the modified couple stress theory in conjunction with the Timoshenko beam model, again including surface effects. Other studies addressed wave propagation in periodic planar beam lattices of different forms, using the so-called modified couple stress theory with an enhanced shear-deformable beam model (Mancusi et al., 2017) or with the Euler-Bernoulli beam model (Sepehri et al., 2021) and, alternatively, using the stress-driven nonlocal theory with the Rayleigh beam model (Russillo and Failla, 2022).

Although several results may be found in literature on wave propagation in small-size beams modelled by nonlocal or generalized continuum theories, a few only concern the recently introduced stress-driven nonlocal theory (Barretta et al., 2024; Russillo and Failla, 2022), with applications limited to beams and beam lattices modelled by the Euler-Bernoulli beam model (Barretta et al., 2024) and the Rayleigh beam model (Russillo and Failla, 2022), respectively. To fill this gap and further investigate into the potential of the stress-driven nonlocal theory, this work deals with wave propagation in small-size beams proposing a stress-driven nonlocal Timoshenko beam formulation and developing an original analytical/computational framework for bare and periodic beams, not yet available for small-size beams modelled by the stress-driven nonlocal theory.

Both infinite and finite beams are addressed in the proposed framework, which delivers the following main novelties. First, the dispersion curves of the bare beam are obtained by exact analytical expressions, providing full insight into the effects of nonlocality. Second, an exact Plane Wave Expansion (PWE) method is formulated to study periodic beams, either equipped with mass-spring resonators or resting on elastic supports; notably, both $\omega(q)$ and $q(\omega)$ dispersion curves are derived, where ω is the frequency and q is the wave number. Third, an approximate homogenization approach is introduced, which estimates opening frequencies and sizes of band gaps induced by mass-spring resonators. Finally, a two-field finite element method, involving displacements and stresses, is developed to calculate the transmittance of finite periodic beams. While the wave solutions/methods for infinite beams (i.e., dispersion curves of bare beam, PWE method and homogenization approach for periodic beams) are built from the differential formulation of the stress-driven nonlocal model, the two-field finite element method for finite periodic beams relies on its integral formulation.

Numerical applications investigate the dispersion diagram of bare and periodic beams for different internal lengths of the stress-driven nonlocal model. Results for finite periodic beams validate the predictions from wave propagation analysis of corresponding infinite ones. This is a remarkable conclusion of this work, which demonstrates the correctness of the proposed PWE method, homogenization approach and two-field finite element method, as well as the theoretical consistency between the differential formulation of the stress-driven nonlocal model used for infinite beams and its integral formulation used for finite ones. Moreover, parametric analyses of periodic beams on elastic supports show the capability of the stress-driven nonlocal model in capturing small-size effects.

The paper is organized as follows. Section 2 introduces the basic concepts of the stress-driven nonlocal Timoshenko beam formulation. Wave propagation analysis is addressed in Section 3, Section 4 and

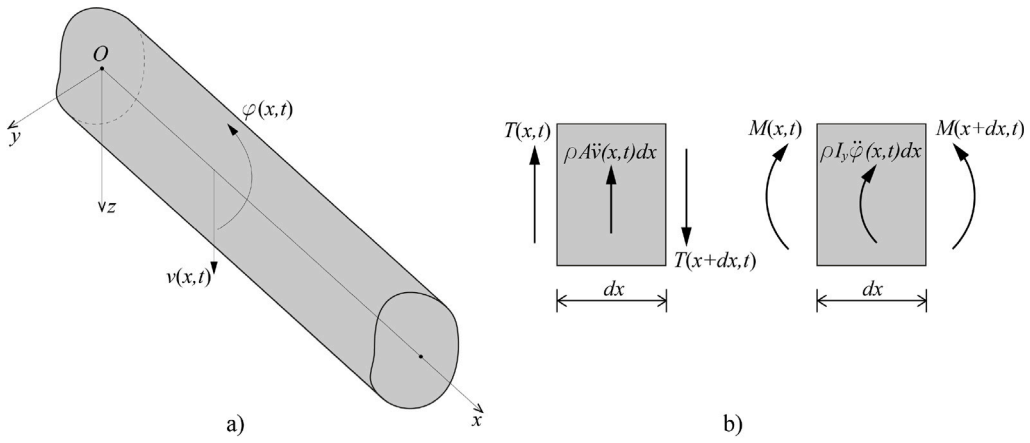

Fig. 1. Stress-driven nonlocal Timoshenko beam: (a) outline; (b) equilibrium in z-direction and about y-axis. Positive sign conventions are shown. Inertial force/moment in (b) are those associated with positive accelerations, according to D'Alembert principle.

Section 5, introducing the exact analytical expressions for the dispersion curves of the bare beam in Section 3 and the PWE method for periodic beams in Section 4 and in Section 5. Numerical applications are discussed in Section 6. Finally, Appendix A describes the homogenization approach for periodic beams with mass-spring resonators, while Appendix B illustrates the two-field finite element method to calculate the transmittance of finite periodic beams.

2. Stress-driven nonlocal Timoshenko beam

In this Section, the stress-driven nonlocal Timoshenko beam model used in this study is introduced with appropriate symbology and conventions.

Fig. 1(a) shows a stress-driven nonlocal Timoshenko beam with arbitrary cross section. In the Cartesian orthogonal system $O(x, y, z)$, x coincides with the centroidal axis of the beam, y and z are principal axes of the cross section. Focusing on the flexural response in the xz plane, $v(x,t)$ and $\varphi(x,t)$ denote deflection in the z-direction and rotation of the cross section about the y-axis (positive sign conventions in Fig. 1(a)).

Generalized strains and displacements of the beam cross section are related by the following equations:

$$\gamma(x,t) = v^{(1)}(x) + \varphi(x,t) \tag{1a}$$

$$\chi(x,t) = \varphi^{(1)}(x,t) \tag{1b}$$

where $\gamma(x,t)$ is the shear strain, $\chi(x,t)$ is the curvature and the superscript (j) means jth derivative with respect to x.

The stress-driven nonlocal Timoshenko beam model formulated in this work relies on the following integral constitutive laws for shear and bending responses:

$$\gamma(x,t) = \frac{1}{GA_s}\int_a^b \Phi(x,\xi)T(\xi,t)d\xi \tag{2a}$$

$$\chi(x,t) = \frac{1}{EI_y}\int_a^b \Phi(x,\xi)M(\xi,t)d\xi \tag{2b}$$

with a and b the lower/upper bounds of the beam domain, ξ an auxiliary longitudinal spatial coordinate, A_s the shear area of the cross section, I_y the moment of inertia of the cross section about the y-axis, G the shear elastic modulus, E the Young's modulus, $T(x,t)$ the shear force, $M(x,t)$ the bending moment about the y-axis, $\Phi(x)$ the attenuation function that is characterized by positivity, symmetry and impulsivity (Romano and Barretta, 2017a). A convenient and commonly used form of the attenuation function is the bi-exponential one (Romano and Barretta, 2017a)

$$\Phi(x,\xi) = \frac{1}{2\lambda}\exp\left(-\frac{|x-\xi|}{\lambda}\right) \tag{3}$$

where λ is a material-dependent internal length defining the beam domain where nonlocal interactions are significant. With the choice of the attenuation function in Eq. (3), the integral constitutive laws in Eqs. (2) can be reverted to the following equivalent differential equations:

$$\gamma(x,t) - \lambda^2\gamma^{(2)}(x,t) = \frac{T(x,t)}{GA_s} \tag{4a}$$

$$\chi(x,t) - \lambda^2\chi^{(2)}(x,t) = \frac{M(x,t)}{EI_y} \tag{4b}$$

complemented by the following constitutive boundary conditions (BCs):

$$\zeta^{(1)}(a,t) = \frac{1}{\lambda}\zeta(a,t) \tag{5a}$$

$$\zeta^{(1)}(b,t) = -\frac{1}{\lambda}\zeta(b,t) \tag{5b}$$

with $\zeta \equiv \gamma$ for the constitutive BCs related to Eq. (4a), while $\zeta \equiv \chi$ for the constitutive BCs related to Eq. (4b).

Next, consider the dynamic equilibrium equations of the beam in the z-direction and about the y-axis (see Fig. 1(b))

$$T^{(1)}(x,t) - \rho A\ddot{v}(x,t) = 0 \tag{6a}$$

$$M^{(1)}(x,t) - T(x,t) - \rho I_y\ddot{\varphi}(x,t) = 0 \tag{6b}$$

where dot means time derivative. By combining Eqs. (4) with Eqs. (6) and considering Eq. (1a), the following partial differential equations governing the flexural vibrations of the stress-driven nonlocal Timoshenko beam are obtained:

$$-\left[\left(v^{(2)}(x,t) + \varphi^{(1)}(x,t)\right) - \lambda^2\left(v^{(4)}(x,t) + \varphi^{(3)}(x,t)\right)\right] + \alpha\ddot{v}(x,t) = 0 \tag{7a}$$

$$-\left(\varphi^{(2)}(x,t) - \lambda^2\varphi^{(4)}(x,t)\right) + \beta\left[\left(v^{(1)}(x,t) + \varphi(x,t)\right) - \lambda^2\left(v^{(3)}(x,t) + \varphi^{(2)}(x,t)\right)\right] + \eta\ddot{\varphi}(x,t) = 0 \tag{7b}$$

with

$$\alpha = \frac{\rho A}{GA_s} \qquad \beta = \frac{GA_s}{EI_y} \qquad \eta = \frac{\rho}{E} \tag{8}$$

It is worthwhile noting that, as the internal length $\lambda \to 0$, Eqs. (7) revert to the system of partial differential equations governing the flexural vibrations of the classical local Timoshenko beam. The solution of Eqs. (7) is obtained by applying four standard mechanical/kinematic BCs at the beam ends and the constitutive BCs in Eqs. (5). The BCs are relevant in the dynamic analysis of beams of finite length but not in the elastic wave propagation analysis of infinite beams, which is pursued in the following Section 3, Section 4 and Section 5. In this respect, see

the work in Barretta et al. (2024), where the characteristic equation for wave propagation analysis in infinite stress-driven nonlocal beams is obtained from the equilibrium differential equations only, without considering any boundary conditions.

3. Wave propagation in stress-driven nonlocal Timoshenko beam

For wave propagation analysis of the infinite stress-driven nonlocal Timoshenko beam, the solution of Eqs. (7) is assumed in the typical form

$$v(x,t) = v_0 \mathrm{e}^{\mathrm{i}(\omega t + qx)} \tag{9a}$$

$$\varphi(x,t) = \varphi_0 \mathrm{e}^{\mathrm{i}(\omega t + qx)} \tag{9b}$$

where ω is the circular frequency and q is the wave number. Substituting Eq. (9) for $v(x,t)$ and $\varphi(x,t)$ into Eq. (7) yields

$$\left[q^2\left(1+\lambda^2 q^2\right) - \alpha\omega^2\right] v_0 - \mathrm{i}q\left(1+\lambda^2 q^2\right)\varphi_0 = 0 \tag{10a}$$

$$\mathrm{i}\beta q\left(1+\lambda^2 q^2\right) v_0 + \left[\left(q^2+\beta\right)\left(1+\lambda^2 q^2\right) - \eta\omega^2\right]\varphi_0 = 0 \tag{10b}$$

with i the imaginary unit. The system in Eqs. (10) is recast in the following compact form:

$$\mathbf{A}\mathbf{d}_0 = \mathbf{0} \tag{11}$$

where $\mathbf{d}_0 = [v_0\ \varphi_0]^T$ and

$$\mathbf{A} = \begin{bmatrix} q^2\left(1+\lambda^2 q^2\right) - \alpha\omega^2 & -iq\left(1+\lambda^2 q^2\right) \\ i\beta q\left(1+\lambda^2 q^2\right) & \left(q^2+\beta\right)\left(1+\lambda^2 q^2\right) - \eta\omega^2 \end{bmatrix} \tag{12}$$

Solutions $\omega(q)$ correspond to non-trivial solutions $\mathbf{d}_0$ of Eq. (12), obtained by setting $\det \mathbf{A} = 0$ in the following form:

$$a_4\omega^4 + a_2\omega^2 + a_0 = 0 \tag{13a}$$

$$a_4 = \alpha\eta \tag{13b}$$

$$a_2 = -\left[\alpha\beta + q^2(\alpha+\eta)\right]\left(1+\lambda^2 q^2\right) \tag{13c}$$

$$a_0 = q^4\left(1+\lambda^2 q^2\right)^2 \tag{13d}$$

Remarkably, Eq. (13a) provides closed-form analytical expressions $\omega(q)$ given by:

$$\omega_{1,2}(q) = \pm\frac{1}{\sqrt{2\alpha\eta}}\sqrt{\left[q^2(\alpha+\eta) + \alpha\beta - c_1\right]\left(1+q^2\lambda^2\right)} \tag{14a}$$

$$\omega_{3,4}(q) = \pm\frac{1}{\sqrt{2\alpha\eta}}\sqrt{\left[q^2(\alpha+\eta) + \alpha\beta + c_1\right]\left(1+q^2\lambda^2\right)} \tag{14b}$$

$$c_1 = \sqrt{q^4(\alpha-\eta)^2 + 2q^2\alpha\beta(\alpha+\eta) + \alpha^2\beta^2} \tag{14c}$$

Eqs. (14) demonstrates that $\omega_{1,2}(q)$ and $\omega_{3,4}(q)$ depend on the parameter $q^2\lambda^2 = (2\pi\lambda/l)^2$, i.e., on the ratio of the material-dependent internal length λ to the wavelength l of the travelling wave. It is evident from Eqs. (14) that, for given λ characterizing the material, nonlocal effects will become significant as l is comparable with or is smaller than λ, while they will reduce and eventually vanish as l is very large with respect to λ. This behaviour substantiates the stress-driven nonlocal model as a physically consistent phenomenological approach to account for microstructural effects on elastic wave propagation. Indeed, microstructural effects are expected to be relevant in waves with $l \lesssim \lambda$, while they are expected to vanish if $l > \lambda$, which is the range of validity of classical local continuum mechanics.

Eqs. (14) allow a full insight into the wave dispersion properties of the stress-driven nonlocal Timoshenko beam and, to the best of authors' knowledge, are not yet available. Obviously, for numerical purposes, only the positive roots $\omega_1(q)$ and $\omega_3(q)$ in Eq. (14) will be considered in the following.

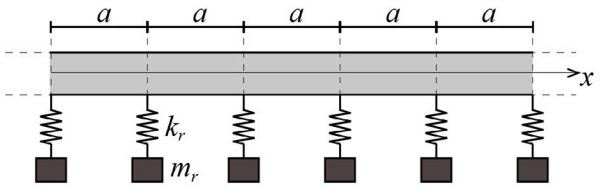

Fig. 2. Periodic stress-driven nonlocal Timoshenko beam with mass-spring resonators.

4. Wave propagation in periodic stress-driven nonlocal Timoshenko beam with mass-spring resonators

Building on the concepts introduced in Section 3, this Section addresses the wave propagation analysis of infinite stress-driven nonlocal Timoshenko beams equipped with periodically spaced mass-spring resonators, as shown in Fig. 2. Wave propagation analysis of nonlocal beams with periodically spaced mass-spring resonators gained attention in recent studies (Trabelssi et al., 2024), because periodicity and local resonance may induce band gaps, i.e., frequency ranges where elastic waves cannot propagate, with benefits in terms of vibration reduction. Consistently with the literature in the field (Xiao et al., 2012), the mass-spring resonators in Fig. 2 may model resonant units attached externally to the beam.

Let m_r be the mass and k_r the stiffness of the resonators. They are located at $x_j = x_0 + ja$, with $j \in \mathbb{Z}$, where $x_0 = a/2$ is a reference abscissa and a the distance between two consecutive resonators.

The dynamic equilibrium equations of the beam-resonators coupled system read

$$-\left[\left(v^{(2)}(x,t) + \varphi^{(1)}(x,t)\right) - \lambda^2\left(v^{(4)}(x,t) + \varphi^{(3)}(x,t)\right)\right] + \\ + \alpha\ddot{v}(x,t) - \sum_{j=-\infty}^{\infty}\kappa_r\left(w_j(t) - v(x_j,t)\right)\delta\ (x-x_j) = 0 \tag{15a}$$

$$-\left(\varphi^{(2)}(x,t) - \lambda^2\varphi^{(4)}(x,t)\right) + \beta\left[\left(v^{(1)}(x,t) + \varphi(x,t)\right) + \\ - \lambda^2\left(v^{(3)}(x,t) + \varphi^{(2)}(x,t)\right)\right] + \eta\ \ddot{\varphi}(x,t) = 0 \tag{15b}$$

$$-k_r\left(v(x_j,t) - w_j(t)\right) + m_r\ddot{w}_j(t) = 0 \tag{15c}$$

where $\kappa_r = k_r/(GA_s)$, $w_j(t)$ is the displacement along the z-direction of the resonator located at x_j and $\delta(x)$ is the Dirac's delta function. The Dirac's deltas in Eq. (15a) capture the shear-force discontinuities caused by the concentrated reaction forces of the mass-spring resonators, as shown in previous studies on local and nonlocal beam models (Wang and Shindo, 2006; Wang and Liew, 2007; Russillo and Failla, 2022; Caporale et al., 2022). Notice that, since Dirac's deltas are used in Eq. (15a), no additional constitutive conditions accounting for shear-force discontinuities shall be considered at the application points of the mass-spring resonators, as discussed in Caporale et al. (2022).

For wave propagation analysis, the solutions of Eqs. (15) take the form

$$v(x,t) = \overline{v}(x)\exp(\mathrm{i}\omega t)\,; \quad \varphi(x,t) = \overline{\varphi}(x)\exp(\mathrm{i}\omega t)\,; \quad w_j(t) = \overline{w}_j\exp(\mathrm{i}\omega t) \tag{16}$$

Substituting Eqs. (16) for $v(x,t)$, $\varphi(x,t)$ and $w_j(t)$ into Eqs. (15) gives

$$-\left[\left(\overline{v}^{(2)}(x) + \overline{\varphi}^{(1)}(x)\right) - \lambda^2\left(\overline{v}^{(4)}(x) + \overline{\varphi}^{(3)}(x)\right)\right] + \\ - \alpha\omega^2\overline{v}(x) - \sum_{j=-\infty}^{\infty}\kappa_r\left(\overline{w}_j - \overline{v}(x_j)\right)\ \delta(x-x_j) = 0 \tag{17a}$$

$$-\left(\overline{\varphi}^{(2)}(x) - \lambda^2\overline{\varphi}^{(4)}(x)\right) + \beta\left[\left(\overline{v}^{(1)}(x) + \overline{\varphi}(x)\right) + \\ - \lambda^2\left(\overline{v}^{(3)}(x) + \overline{\varphi}^{(2)}(x)\right)\right] - \eta\omega^2\overline{\varphi}(x) = 0 \tag{17b}$$

$$-k_r\left(\overline{v}(x_j)-\overline{w}_j\right)-m_r\omega^2\overline{w}_j=0 \tag{17c}$$

As explained in the following, here Eqs. (17) are solved by the PWE method, which consists in adopting a suitable Fourier series expansion for the unknown generalized displacements (deflection, rotation) defined over the whole domain of the infinite beam. This method is ideally suitable for the problem under study, as it preserves the nonlocal interactions between points belonging to different cells, including non-adjacent ones, without introducing any approximation. To the best of authors' knowledge, this study is the first to apply the PWE method for wave propagation analysis of stress-driven nonlocal beams. Remarkably, both the $\omega(q)$ and the $q(\omega)$ methods can be derived by the proposed PWE formulation, as detailed below.

4.1. $\omega(q)$ method

In the $\omega(q)$ method, the wave dispersion curves are obtained from an eigenvalue problem providing the frequencies ω that correspond to wave numbers q within the irreducible Brillouin zone $[0,\pi/a]$.

According to the PWE method, the solutions $\overline{v}$ and $\overline{\varphi}$ of Eqs. (17) are represented in the form

$$\overline{v}(x)=\sum_{m=-\infty}^{\infty}v_m e^{i(q+2m\pi/a)x} \tag{18a}$$

$$\overline{\varphi}(x)=\sum_{m=-\infty}^{\infty}\varphi_m e^{i(q+2m\pi/a)x} \tag{18b}$$

Further, given the periodicity of the beam, the Bloch theorem guarantees that

$$\overline{v}(x_j)=\overline{v}(x_0)e^{-iqja} \tag{19a}$$

$$\overline{\varphi}(x_j)=\overline{\varphi}(x_0)e^{-iqja} \tag{19b}$$

$$\overline{w}_j=\overline{w}_0 e^{-iqja} \tag{19c}$$

Replacing Eqs. (19) for $\overline{v}$, $\overline{\varphi}$ and $\overline{w}_j$ in Eqs. (17) yields an infinite set of systems of algebraic equations, each system corresponding to a value $m=-\infty,\dots,\infty$:

$$\left[q_m^2\left(1+\lambda^2q_m^2\right)-\alpha\omega^2\right]v_m-iq_m\left(1+\lambda^2q_m^2\right)\varphi_m+ -\overline{\kappa}_r\left(w_0-\sum_{\tilde{m}=-\infty}^{\infty}v_{\tilde{m}}e^{-i(q+2\tilde{m}\pi/a)x_0}\right)e^{i(q+2m\pi/a)x_0}=0 \tag{20a}$$

$$i\beta q_m\left(1+\lambda^2q_m^2\right)v_m+\left[\left(q_m^2+\beta\right)\left(1+\lambda^2q_m^2\right)-\eta\omega^2\right]\varphi_m=0 \tag{20b}$$

$$-k_r\left(\sum_{\tilde{m}=-\infty}^{\infty}v_{\tilde{m}}e^{-i(q+2\tilde{m}\pi/a)x_0}-w_0\right)-m_r\omega^2w_0=0 \tag{20c}$$

where $\overline{\kappa}_r=\kappa_r/a$ and $q_m=q+2\pi m/a$. Eqs. (20) are obtained by some manipulations, as detailed below:

(i) Exploiting the sampling property of the Dirac's delta function, the following identity holds:

$$\sum_{j=-\infty}^{\infty}e^{-iqja}\delta(x-x_j)=e^{-iq(x-x_0)}\sum_{j=-\infty}^{\infty}\delta(x-x_j) \tag{21}$$

(ii) Being the summation of Dirac's delta functions in Eq. (21) a periodic function, the following expression can be adopted:

$$\sum_{j=-\infty}^{\infty}\delta(x-x_j)=\frac{1}{a}\sum_{m=-\infty}^{\infty}e^{i(2m\pi/a)x_0}e^{-i(2m\pi/a)x} \tag{22}$$

(iii) In view of Eq. (18a), the deflection at $x=x_0$ can be recast in the following form:

$$\overline{v}(x_0)=\sum_{\tilde{m}=-\infty}^{\infty}v_{\tilde{m}}e^{-i(q+2\tilde{m}\pi/a)x_0} \tag{23}$$

To build a solution, the summation over the indexes m in Eqs. (18) and $\tilde{m}$ in Eqs. (20) are truncated to a finite order, i.e., $m,\tilde{m}=-M,-M+1,\dots,M-1,M$. As a result, a system of $4M+3$ equations is obtained, where $2M+1=\overline{M}$ equations are of the type in Eq. (20a), $2M+1=\overline{M}$ equations are of the type in Eq. (20b) and one is Eq. (20c). This system can be cast in matrix form as

$$\left(\mathbf{K}-\omega^2\mathbf{M}\right)\mathbf{d}_M^*=\mathbf{0} \tag{24}$$

where $\mathbf{d}_M^*=\left[\mathbf{v}_M^T\ \boldsymbol{\varphi}_M^T\ w_0\right]^T$, with $\mathbf{v}_M^T=\left[v_{-M}\ \dots\ v_M\right]$, $\boldsymbol{\varphi}_M^T=\left[\varphi_{-M}\ \dots\ \varphi_M\right]$ and

$$\mathbf{K}=\begin{bmatrix}\mathbf{Q}_2+\lambda^2\mathbf{Q}_4+\overline{\kappa}_r\mathbf{U} & -i\left(\mathbf{Q}_1+\lambda^2\mathbf{Q}_3\right) & -\overline{\kappa}_r\mathbf{p}\\ i\beta\left(\mathbf{Q}_1+\lambda^2\mathbf{Q}_3\right) & \beta\left(\mathbf{I}+\lambda^2\mathbf{Q}_2\right)+\mathbf{Q}_2+\lambda^2\mathbf{Q}_4 & \mathbf{z}\\ -k_r\mathbf{p}' & \mathbf{z}^T & k_r\end{bmatrix} \tag{25a}$$

$$\mathbf{M}=\begin{bmatrix}\alpha\mathbf{I} & \mathbf{Z} & \mathbf{z}\\ \mathbf{Z} & \eta\mathbf{I} & \mathbf{z}\\ \mathbf{z}^T & \mathbf{z}^T & m_r\end{bmatrix} \tag{25b}$$

In Eqs. (25) $\mathbf{I}$ is a $\overline{M}\times\overline{M}$ identity matrix, $\mathbf{z}$ is a $\overline{M}$ column vector with all entries equal to zero, $\mathbf{Z}=\mathbf{z}\mathbf{z}^T$, $\mathbf{U}=\mathbf{p}\mathbf{p}'$ and

$$\mathbf{Q}_n=\begin{bmatrix}(q-2M\pi/a)^n & 0 & \cdots & 0\\ 0 & \left[q-2(M-1)\pi/a\right]^n & \cdots & \vdots\\ \vdots & \vdots & \ddots & 0\\ 0 & \cdots & 0 & (q+2M\pi/a)^n\end{bmatrix} \tag{26a}$$

$$\mathbf{p}=\begin{bmatrix}e^{i(q-2M\pi/a)x_0}\\ e^{i[q-2(M-1)\pi/a]x_0}\\ \vdots\\ e^{i(q+2M\pi/a)x_0}\end{bmatrix} \tag{26b}$$

$$\mathbf{p}'=\begin{bmatrix}e^{-i(q-2M\pi/a)x_0}\\ e^{-i[q-2(M-1)\pi/a]x_0}\\ \vdots\\ e^{-i(q+2M\pi/a)x_0}\end{bmatrix}^T \tag{26c}$$

Eq. (24) defines a linear generalized eigenvalue problem in ω^2, from which the frequencies $\omega(q)$ corresponding to each wave number $q\in[0,\pi/a]$ are obtained. The solutions $\omega(q)$ are real valued; band gaps occur in frequency ranges where no eigenvalues exist.

4.2. $q(\omega)$ method

To formulate the $q(\omega)$ method, it is convenient to express the reaction force of each resonator as function of its dynamic stiffness. It follows that Eqs. (20) are rewritten as

$$-\left[\left(\overline{v}^{(2)}(x)+\overline{\varphi}^{(1)}(x)\right)-\lambda^2\left(\overline{v}^{(4)}(x)+\overline{\varphi}^{(3)}(x)\right)\right]+ -\alpha\omega^2\overline{v}(x)+\kappa_{Dr}(\omega)\sum_{j=-\infty}^{\infty}\overline{v}(x_j)\delta(x-x_j)=0 \tag{27a}$$

$$-\left(\overline{\varphi}^{(2)}(x)-\lambda^2\overline{\varphi}^{(4)}(x)\right)+\beta\left[\left(\overline{v}^{(1)}(x)+\overline{\varphi}(x)\right) -\lambda^2\left(\overline{v}^{(3)}(x)+\overline{\varphi}^{(2)}(x)\right)\right]-\eta\omega^2\overline{\varphi}(x)=0 \tag{27b}$$

where $\kappa_{Dr}(\omega) = k_{Dr}(\omega)/(GA_s)$ and

$$k_{Dr}(\omega) = \frac{k_r m_r \omega^2}{m_r \omega^2 - k_r} \tag{28}$$

is the dynamic stiffness of the resonator. Considering Eq. (21) through Eq. (23), an infinite set of systems of algebraic equations of the following type is obtained:

$$\left[q_m^2\left(1+\lambda^2 q_m^2\right) - \alpha\omega^2\right] v_m \; -\mathrm{i} q_m \left(1+\lambda^2 q_m^2\right)\varphi_m + \\ + \overline{\kappa}_{Dr}\,(\omega) \sum_{\tilde{m}=-\infty}^{\infty} \mathrm{e}^{-\mathrm{i}(2\tilde{m}\pi/a)x_0}\,\mathrm{e}^{\mathrm{i}(q+2m\pi/a)x_0} v_{\tilde{m}} = 0 \tag{29a}$$

$$\mathrm{i}\beta q_m \left(1+\lambda^2 q_m^2\right) v_m + \left[\left(q_m^2+\beta\right)\left(1+\lambda^2 q_m^2\right) - \eta\omega^2\right]\varphi_m = 0 \tag{29b}$$

with $\overline{\kappa}_{Dr}(\omega) = \kappa_{Dr}(\omega)/a$. The summations over the indexes m in Eqs. (18) and $\tilde{m}$ in Eqs. (29) can be truncated to a finite order, i.e., $m, \tilde{m} = -M, -M+1, \ldots, M-1, M$, obtaining a system of $4M+2 = 2\overline{M}$ algebraic equations of type (29), written in compact form as

$$\mathbf{D}\mathbf{d}_M = \mathbf{0} \tag{30}$$

$$\mathbf{D} = \begin{bmatrix} \mathbf{Q}_2 + \lambda^2\mathbf{Q}_4 + \overline{\kappa}_{Dr}(\omega)\mathbf{H} - \alpha\omega^2\mathbf{I} & -i\left(\mathbf{Q}_1 + \lambda^2\mathbf{Q}_3\right) \\ i\beta\left(\mathbf{Q}_1 + \lambda^2\mathbf{Q}_3\right) & \beta\left(\mathbf{I} + \lambda^2\mathbf{Q}_2\right) + \left(\mathbf{Q}_2 + \lambda^2\mathbf{Q}_4\right) - \eta\omega^2\mathbf{I} \end{bmatrix} \tag{31}$$

where $\mathbf{d}_M = \begin{bmatrix}\mathbf{v}_M^T & \boldsymbol{\varphi}_M^T\end{bmatrix}^T$, $\mathbf{H} = \mathbf{r}\mathbf{r}'$ with

$$\mathbf{r} = \begin{bmatrix} \mathrm{e}^{\mathrm{i}(-2M\pi/a)x_0} \\ \mathrm{e}^{\mathrm{i}[-2(M-1)\pi/a]x_0} \\ \vdots \\ \mathrm{e}^{\mathrm{i}(2M\pi/a)x_0} \end{bmatrix} \tag{32a}$$

$$\mathbf{r}' = \begin{bmatrix} \mathrm{e}^{-\mathrm{i}(-2M\pi/a)x_0} \\ \mathrm{e}^{-\mathrm{i}[-2(M-1)\pi/a]x_0} \\ \vdots \\ \mathrm{e}^{-\mathrm{i}(2M\pi/a)x_0} \end{bmatrix}^T \tag{32b}$$

The matrices $\mathbf{Q}_j$ in Eq. (31), with $j = 1,2,3,4$, are given by Eq. (26a). Terms of $\mathbf{Q}_j$ can be expanded as

$$q_m^4 = (q-2m\pi/a)^4 = \frac{1}{a^4}\left[\overline{q}^4 + p_3(m)\overline{q}^3 + p_2(m)\overline{q}^2 + p_1(m)\overline{q} + p_0(m)\right] \tag{33a}$$

$$q_m^3 = (q-2m\pi/a)^3 = \frac{1}{a^3}\left[\overline{q}^3 + r_2(m)\overline{q}^2 + r_1(m)\overline{q} + r_0(m)\right] \tag{33b}$$

$$q_m^2 = (q-2m\pi/a)^2 = \frac{1}{a^2}\left[\overline{q}^2 + s_1(m)\overline{q} + s_0(m)\right] \tag{33c}$$

$$q_m = (q-2m\pi/a) = \frac{1}{a}\left[\overline{q} + t_0(m)\right] \tag{33d}$$

with $\overline{q} = qa$ and

$$p_3(m) = -8(m\pi); \quad p_2(m) = 24(m\pi)^2; \quad p_1(m) = -32(m\pi)^3; \quad p_0(m) = 16(m\pi)^4 \tag{34a}$$

$$r_2(m) = -6(m\pi); \quad r_1(m) = 12(m\pi)^2; \quad r_0(m) = -8(m\pi)^3 \tag{34b}$$

$$s_1(m) = -4(m\pi); \quad s_0(m) = 4(m\pi)^2 \tag{34c}$$

$$t_0(m) = -2(m\pi) \tag{34d}$$

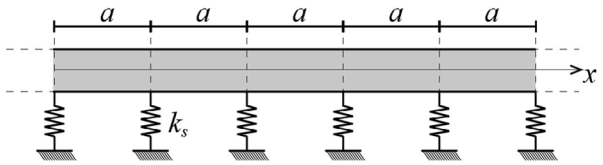

Fig. 3. Periodic stress-driven nonlocal Timoshenko beam on elastic supports.

It follows that the matrices $\mathbf{Q}_j$, with $j = 1,2,3,4$, can be rewritten as

$$\mathbf{Q}_4 = \frac{1}{a^4}\left[\overline{q}^4\mathbf{I} + \overline{q}^3\mathbf{P}_3 + \overline{q}^2\mathbf{P}_2 + \overline{q}\mathbf{P}_1 + \mathbf{P}_0\right] \tag{35a}$$

$$\mathbf{Q}_3 = \frac{1}{a^3}\left[\overline{q}^3\mathbf{I} + \overline{q}^2\mathbf{R}_2 + \overline{q}\mathbf{R}_1 + \mathbf{R}_0\right] \tag{35b}$$

$$\mathbf{Q}_2 = \frac{1}{a^2}\left[\overline{q}^2\mathbf{I} + \overline{q}\mathbf{S}_1 + \mathbf{S}_0\right] \tag{35c}$$

$$\mathbf{Q}_1 = \frac{1}{a}\left[\overline{q}\mathbf{I} + \mathbf{T}_0\right] \tag{35d}$$

Symbols $\mathbf{P}_n$, $\mathbf{R}_n$, $\mathbf{S}_n$ and $\mathbf{T}_0$ in Eqs. (35) denote matrices deriving from the general form

$$\boldsymbol{\Theta}_n = \begin{bmatrix} \theta_n(-M) & 0 & \cdots & 0 \\ 0 & \theta_n(-M+1) & \cdots & \vdots \\ \vdots & \vdots & \ddots & 0 \\ 0 & \cdots & 0 & \theta_n(M) \end{bmatrix} \tag{36}$$

with $\theta_n \equiv p_n$ for $\boldsymbol{\Theta}_n \equiv \mathbf{P}_n$, $\theta_n \equiv r_n$ for $\boldsymbol{\Theta}_n \equiv \mathbf{R}_n$, $\theta_n \equiv s_n$ for $\boldsymbol{\Theta}_n \equiv \mathbf{S}_n$ and $\theta_0 \equiv t_0$ for $\boldsymbol{\Theta}_0 \equiv \mathbf{T}_0$; p_n, r_n, s_n and t_0 are given in Eqs. (34).

Considering Eqs. (35), Eq. (30) can be rewritten as

$$\left(\overline{q}^4\mathbf{I}_{2\overline{M}} + \overline{q}^3\mathbf{A}_3 + \overline{q}^2\mathbf{A}_2 + \overline{q}\mathbf{A}_1 + \mathbf{A}_0\right)\mathbf{d}_M = \mathbf{0} \tag{37}$$

where $\mathbf{I}_{2\overline{M}}$ is a $2\overline{M}\times 2\overline{M}$ identity matrix and

$$\mathbf{A}_3 = \begin{bmatrix} \lambda^2\mathbf{P}_3 & -ia\mathbf{I} \\ ia\beta\mathbf{I} & \mathbf{P}_3 \end{bmatrix} \tag{38a}$$

$$\mathbf{A}_2 = \begin{bmatrix} \lambda^2\mathbf{P}_2 + a^2\mathbf{I} & -ia\lambda^2\mathbf{R}_2 \\ ia\beta\lambda^2\mathbf{R}_2 & \lambda^2\mathbf{P}_2 + a^2\mathbf{I} + a^2\beta\mathbf{I} \end{bmatrix} \tag{38b}$$

$$\mathbf{A}_1 = \begin{bmatrix} \lambda^2\mathbf{P}_1 + a^2\mathbf{S}_1 & -ia\left(\lambda^2\mathbf{R}_1 + a^2\mathbf{I}\right) \\ ia\beta\left(\lambda^2\mathbf{R}_1 + a^2\mathbf{I}\right) & \lambda^2\mathbf{P}_1 + a^2\mathbf{S}_1 + a^2\beta\lambda^2\mathbf{S}_1 \end{bmatrix} \tag{38c}$$

$$\mathbf{A}_0 = \begin{bmatrix} \lambda^2\mathbf{P}_0 + a^2\mathbf{S}_0 + \overline{\kappa}_{Dr}(\omega)a^4\mathbf{H} - a^4\alpha\omega^2\mathbf{I} & -ia\left(\lambda^2\mathbf{R}_0 + a^2\mathbf{T}_0\right) \\ ia\beta\left(\lambda^2\mathbf{R}_0 + a^2\mathbf{T}_0\right) & \lambda^2\mathbf{P}_0 + a^2\mathbf{S}_0 + a^2\beta\left(\lambda^2\mathbf{S}_0 + a^2\mathbf{I}\right) - a^4\eta\omega^2\mathbf{I} \end{bmatrix} \tag{38d}$$

The system in Eq. (37) can be recast as a linear standard eigenvalue problem

$$\begin{bmatrix} -\mathbf{A}_3 & -\mathbf{A}_2 & -\mathbf{A}_1 & -\mathbf{A}_0 \\ \mathbf{I}_{2\overline{M}} & \mathbf{Z}_{2\overline{M}} & \mathbf{Z}_{2\overline{M}} & \mathbf{Z}_{2\overline{M}} \\ \mathbf{Z}_{2\overline{M}} & \mathbf{I}_{2\overline{M}} & \mathbf{Z}_{2\overline{M}} & \mathbf{Z}_{2\overline{M}} \\ \mathbf{Z}_{2\overline{M}} & \mathbf{Z}_{2\overline{M}} & \mathbf{I}_{2\overline{M}} & \mathbf{Z}_{2\overline{M}} \end{bmatrix} \begin{bmatrix} \overline{q}^3\mathbf{d}_M \\ \overline{q}^2\mathbf{d}_M \\ \overline{q}\mathbf{d}_M \\ \mathbf{d}_M \end{bmatrix} = \overline{q} \begin{bmatrix} \overline{q}^3\mathbf{d}_M \\ \overline{q}^2\mathbf{d}_M \\ \overline{q}\mathbf{d}_M \\ \mathbf{d}_M \end{bmatrix} \tag{39}$$

where $\mathbf{Z}_{2\overline{M}}$ is a $2\overline{M}\times 2\overline{M}$ matrix of zeros. For each frequency ω, the matrix in Eq. (39) has $8\overline{M}$ eigenvalues $\overline{q}$ that in general are complex valued. Among the $8\overline{M}$ eigenvalues calculated for each frequency ω, only the eigenvalues $\overline{q}$ with $\mathrm{Re}(q) \in [0, \pi/a]$ are considered.

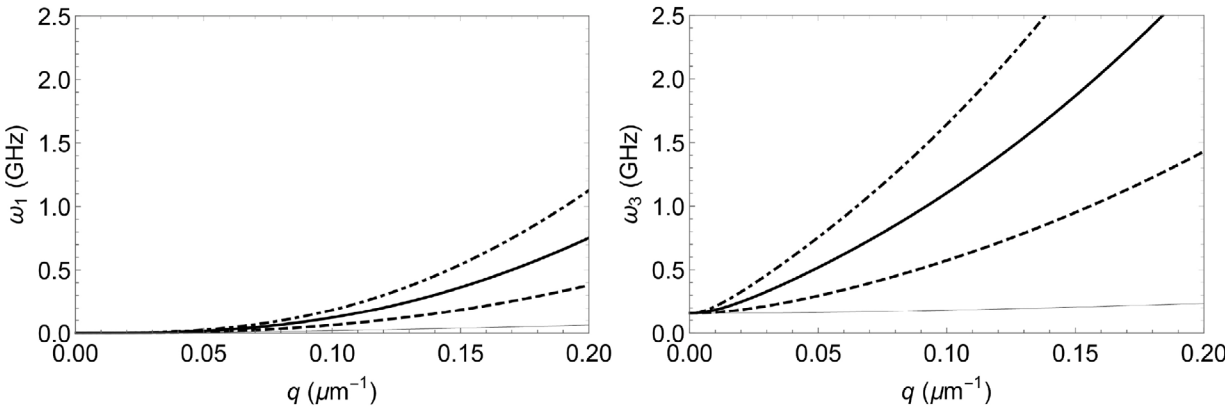

Fig. 4. $\omega(q)$ dispersion curves of bare stress-driven nonlocal Timoshenko microbeam for different internal lengths λ, $\lambda = 0$ (local) thin continuous line, $\lambda = 30$ μm thick dashed line, $\lambda = 60$ μm thick continuous line, $\lambda = 90$ μm thick dot-dashed line; $\omega_1(q)$ in Eq. (14a) (left column); $\omega_3(q)$ in Eq. (14b) (right column).

4.3. Remarks

Remark #1. Here, the formulation of the PWE method is developed for stress-driven nonlocal Timoshenko beams but can readily be extended to Euler-Bernoulli and Rayleigh beams as well. It can also be extended to the case of multiple resonators in every cell, as proposed in Xiao et al. (2012) for local Euler-Bernoulli beams. It handles nonlocal interactions between points belonging to different cells without any restriction and applies, therefore, for any internal length of the stress-driven nonlocal model. It provides the exact dispersion curves to the limit, i.e., increasing the number of terms retained in the Fourier series expansions (18) adopted for deflection and rotation.

Remark #2. For completeness, a homogenization approach is developed in Appendix A, which consists in reverting the discrete distribution of mass-spring resonators to an equivalent continuous one. The homogenization approach is approximate but useful for design, as allows to easily estimate opening frequencies and sizes of local resonance band gaps, as discussed in Appendix A.

5. Wave propagation in periodic stress-driven nonlocal Timoshenko beam on elastic supports

Several studies analysed wave propagation in small-size beams on periodically spaced supports (Allegri et al., 2013; Deng et al., 2017a,b). This Section illustrates how this problem can readily be handled adopting the stress-driven nonlocal Timoshenko beam model as well, by tailoring the PWE method presented in Section 4. Again, it is worthwhile noting that the PWE method is ideally appropriate for this purpose, because it inherently preserves the nonlocal interactions between adjacent and non-adjacent cells, without introducing any approximation. Both the $\omega(q)$ and the $q(\omega)$ methods can be formulated, as explained below.

In the $\omega(q)$ method, the system in Eq. (24) is rewritten as

$$\left(\mathbf{K}_s - \omega^2 \mathbf{M}_s\right) \mathbf{d}_M = \mathbf{0} \tag{40}$$

where

$$\mathbf{K}_s = \begin{bmatrix} \mathbf{Q}_2 + \lambda^2 \mathbf{Q}_4 + \overline{\kappa}_s \mathbf{U} & -i\left(\mathbf{Q}_1 + \lambda^2 \mathbf{Q}_3\right) \\ i\beta\left(\mathbf{Q}_1 + \lambda^2 \mathbf{Q}_3\right) & \beta\left(\mathbf{I} + \lambda^2 \mathbf{Q}_2\right) + \mathbf{Q}_2 + \lambda^2 \mathbf{Q}_4 \end{bmatrix} \tag{41a}$$

$$\mathbf{M}_s = \begin{bmatrix} \alpha \mathbf{I} & \mathbf{Z} \\ \mathbf{Z} & \eta \mathbf{I} \end{bmatrix} \tag{41b}$$

with $\overline{\kappa}_s = k_s/(GA_s a)$. The size of the matrices in Eqs. (41) is $2\overline{M} \times 2\overline{M}$, where $4M + 2 = 2\overline{M}$ and the only generalized coordinates are related to the beam, as no resonators are present. On the other hand, the $q(\omega)$ method can easily be formulated as in Section 4.2, on replacing the dynamic stiffness of the resonator $k_{Dr}(\omega)$ with the constant elastic stiffness of the support k_s.

Both the $\omega(q)$ and the $q(\omega)$ method can handle periodic beams on rigid supports, by selecting a suitably large stiffness of the elastic supports in Fig. 3.

6. Numerical applications

This Section discusses the wave dispersion properties of typical microbeams, modelled as stress-driven nonlocal Timoshenko beams. For a preliminary insight, Section 6.1 deals with a bare microbeam; Section 6.2 focuses on a periodic microbeam equipped with mass-spring resonators, Sections 6.3 and 6.4 address periodic microbeams resting on elastic supports. The analytical solutions derived in Section 3 are applied to the bare microbeam, the PWE method formulated in Sections 4 and 5 and the two-field finite element method developed in Appendix B are applied to the periodic microbeams. For comparison, results for the periodic microbeam with mass-spring resonators are also built by the homogenization approach formulated in Appendix A. In-house codes have been developed in Matlab (MATLAB R2023b, 2022).

6.1. Bare stress-driven nonlocal Timoshenko microbeam

Consider an infinite stress-driven nonlocal Timoshenko microbeam with rectangular cross section and parameters: $H = 10$ μm, $B = 20$ μm, $E = 70$ GPa, $G = 26.3$ GPa, $\rho = 2700$ kg/m^3, where H and B are height and width of the cross section, E the elastic modulus, G the shear modulus, ρ the mass density; the material parameters are those of aluminum (Sepehri et al., 2022). To analyse the influence of nonlocal effects, $\lambda = 0$ μm (local Timoshenko beam), $\lambda = 30$ μm, $\lambda = 60$ μm and $\lambda = 90$ μm are selected for the internal length λ of the stress-driven nonlocal model.

Fig. 4 shows the $\omega_1(q)$ and $\omega_3(q)$ dispersion curves obtained by the analytical solutions (14). First, it is worthwhile noting that the local and nonlocal $\omega_3(q)$ dispersion curves start all from the same cut-off frequency at $q = 0$, i.e., approximately 157 MHz; this is a typical behaviour of the classical local Timoshenko beam model (Ducceschi and Bilbao, 2019) and, remarkably, it is found in the stress-driven nonlocal Timoshenko beam model as well. Further comments are relevant on how the dispersion curves vary with λ: (i) for fixed wave number q, the frequency ω increases with λ, meaning that the response of the microbeam stiffens for increasing λ; interestingly, this result mirrors previous results showing the same stiffening effects in static and dynamic responses of stress-driven nonlocal beams (Russillo and Failla, 2022; Romano and Barretta, 2017a,b; Barretta et al., 2018, 2024; Romano et al., 2017a; Russillo et al., 2021), beam lattices (Russillo and

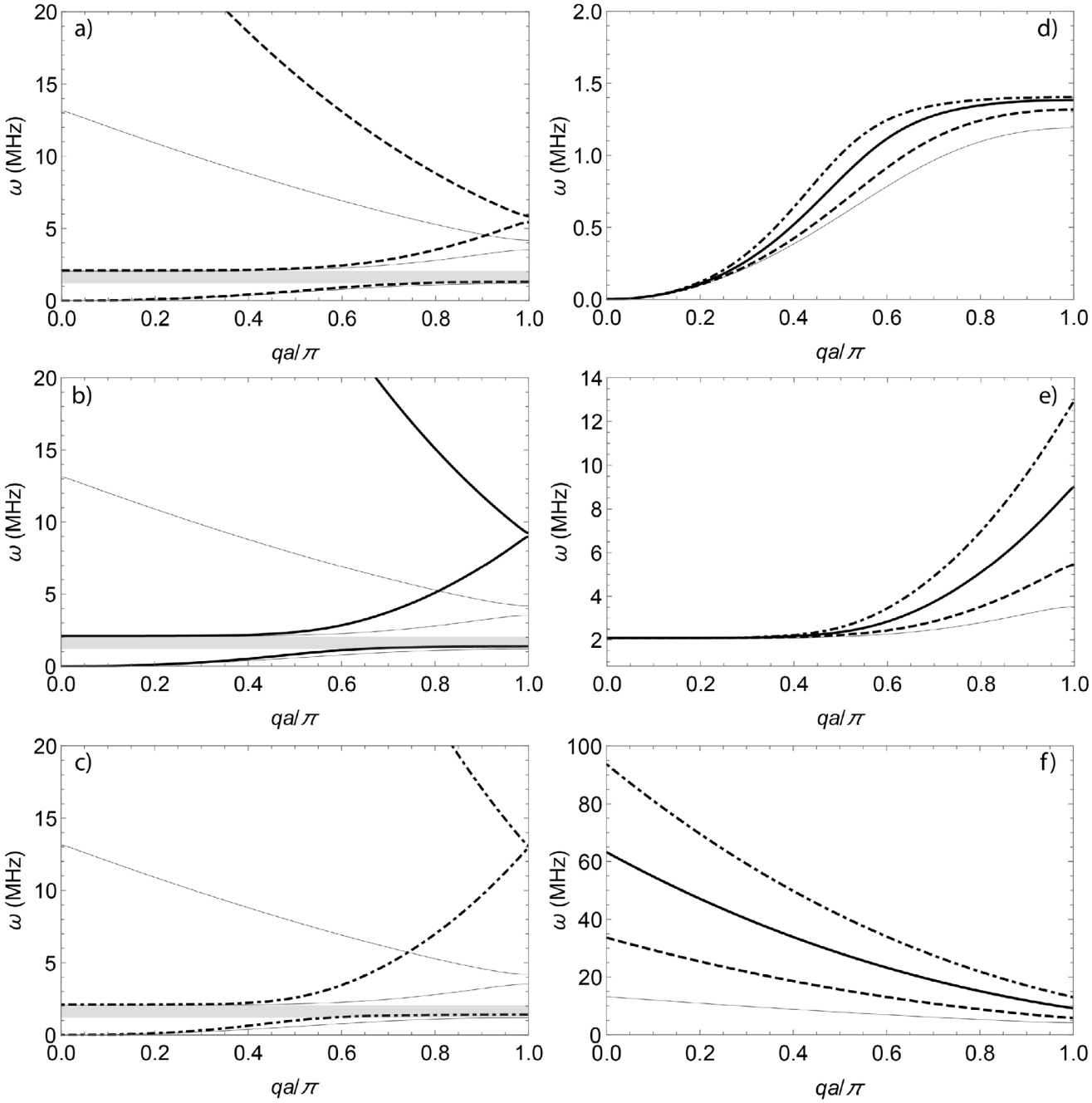

Fig. 5. $\omega(q)$ dispersion curves of periodic stress-driven nonlocal Timoshenko microbeam with mass-spring resonators for different internal lengths λ, $\lambda = 0$ (local) thin continuous line, $\lambda = 30$ μm thick dashed line, $\lambda = 60$ μm thick continuous line, $\lambda = 90$ μm thick dot-dashed line; first three branches for separate values of λ (left column): (a) $\lambda = 0$ and $\lambda = 30$ μm, (b) $\lambda = 0$ and $\lambda = 60$ μm, (c) $\lambda = 0$ and $\lambda = 90$ μm; zoomed view on single branches for all considered values of λ (right column): (d) first branch, (e) second branch, (f) third branch; grey band indicates local resonance band gap for $\lambda = 0$ (local).

Failla, 2022) and plates (Russillo et al., 2022); (ii) for fixed frequency ω, the deviation of the nonlocal response from the local one increases with λ, consistently with the fact that λ is the parameter governing the length of the beam domain where nonlocal effects are relevant. Another important observation is that, for any λ, the deviation of the nonlocal response from the local one is clearly more significant for increasing frequency ω and wave number q, which means decreasing wavelength $l = 2\pi/q$; this behaviour reflects what anticipated in Section 3, i.e., that the deviation of the nonlocal response from the local one is more significant when the wavelength l of the travelling wave is comparable with or is smaller than the internal length λ characterizing the material. As expected, therefore, nonlocal effects are more relevant in the short wavelength/high frequency range.

6.2. Periodic stress-driven nonlocal Timoshenko microbeam with mass-spring resonators

Next, consider an infinite periodic stress-driven nonlocal Timoshenko microbeam with mass-spring resonators, as shown in Fig. 2. The microbeam has the same geometrical and mechanical parameters assumed in Section 6.1 for the bare microbeam. Notice that these parameters are very similar to those used in Sepehri et al. (2022). The

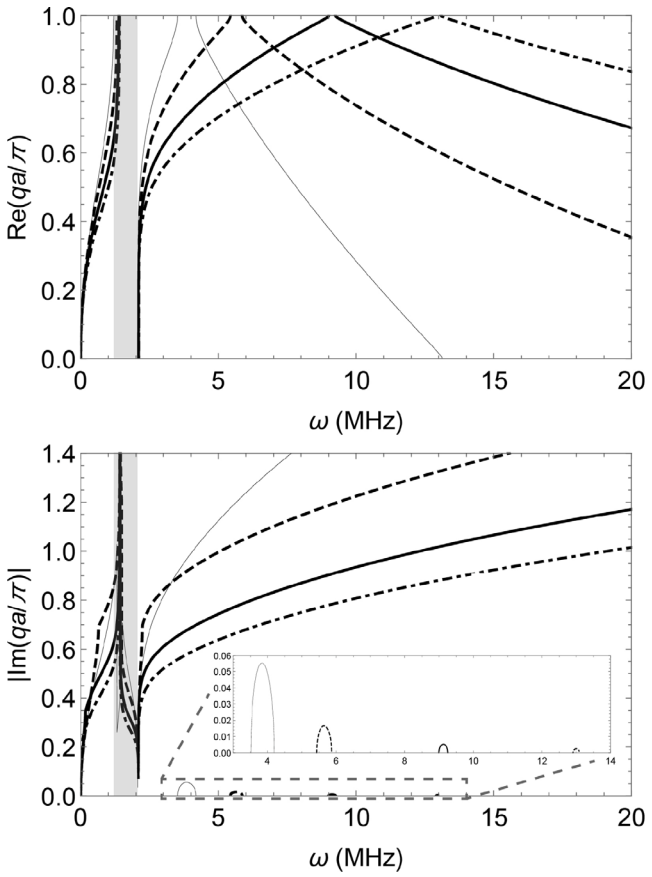

Fig. 6. $q(\omega)$ dispersion curves of periodic stress-driven nonlocal Timoshenko microbeam with mass-spring resonators for different internal lengths λ, $\lambda = 0$ (local) thin continuous line, $\lambda = 30$ μm thick dashed line, $\lambda = 60$ μm thick continuous line, $\lambda = 90$ μm thick dot-dashed line; real parts (top row) and imaginary parts (bottom row); grey band indicates local resonance band gap for $\lambda = 0$ (local).

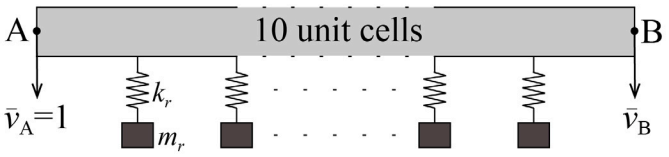

Fig. 7. Finite periodic stress-driven nonlocal Timoshenko microbeam with mass-spring resonators.

resonators are equally spaced at distance $a = 8H = 80$ μm and their properties are mass $m_r = 5{\times}10^{-11}$ kg and stiffness $k_r = 4000$ N/m, which correspond to a tuning frequency $\omega_r = 1.424$ MHz. The influence of nonlocal effects is investigated considering $\lambda = 0$ μm (local Timoshenko beam), $\lambda = 30$ μm, $\lambda = 60$ μm, $\lambda = 90$ μm for the internal length λ, as in Section 6.1; they correspond to $\lambda/a = 0.375, 0.75, 1.125$.

Table 1 reports opening frequency and size of the local resonance band gap, as obtained in Fig. 5 by the PWE method and, for comparison, by the approximate homogenization approach formulated in Appendix A; they are in good agreement, demonstrating that the homogenization approach can reasonably be applied for a first estimate of the opening frequencies and sizes of local resonance band gaps. Fig. 5 shows the $\omega(q)$ dispersion curves obtained by solving the eigenvalue problem in Eq. (24) with $M = 2$. In the considered frequency range, no eigenvalues are found in two separate bands where, therefore, no wave can propagate: the first band is a local resonance band gap, whose opening frequency is slightly below the tuning frequency 1.424 MHz of

Table 1
Opening frequency and size of local resonance band gap for periodic Timoshenko microbeam with mass-spring resonators. OF=Opening Frequency, HO=Homogenization, SZ=Size.

λ (μm)	OF-PWE (MHz)	OF-HO (MHz)	SZ-PWE (MHz)	SZ-HO (MHz)
0	1.190	1.424	0.870	0.667
30	1.317	1.424	0.769	0.667
60	1.383	1.424	0.706	0.667
90	1.404	1.424	0.686	0.667

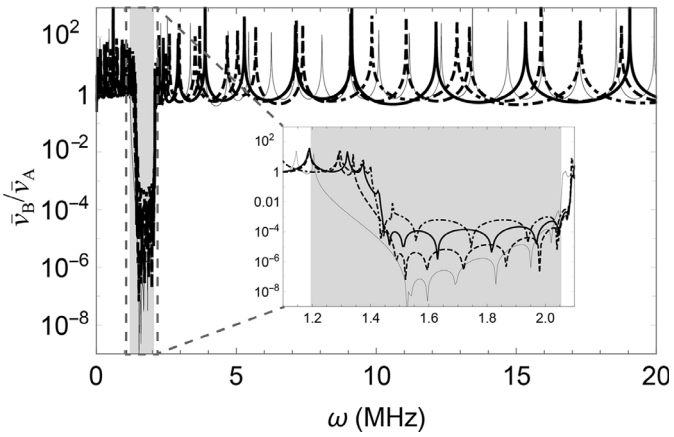

Fig. 8. Transmittance of finite periodic stress-driven nonlocal Timoshenko microbeam with mass-spring resonators in Fig. 7 for different internal lengths λ, $\lambda = 0$ (local) thin continuous line, $\lambda = 30$ μm thick dashed line, $\lambda = 60$ μm thick continuous line, $\lambda = 90$ μm thick dot-dashed line; grey band indicates local resonance band gap for $\lambda = 0$ (local).

the resonators; the second band is a Bragg band gap, whose opening frequency is located in the range 3-13 MHz depending on λ. Focusing on the local resonance band gap, it is observed that its opening frequency slightly increases and the size slightly reduces for increasing λ, while the closing frequency is almost unchanged with λ. Moreover, it is seen that the opening frequency of the Bragg band gap shifts more significantly to higher frequencies and its size reduces for increasing λ as well.

As for the dispersion curves in Fig. 5, it is seen that, for any λ, each nonlocal branch deviates from the corresponding local branch. The deviation of the nonlocal response from the local response becomes more significant for increasing frequency ω, confirming the conclusions drawn from the dispersion curves of the bare microbeam built in Fig. 4 based on Eqs. (14), i.e., nonlocal effects are more relevant in the high frequency range. Indeed, waves at increasing frequency ω feature decreasing wavelength and, as decreasing wavelengths become comparable with or smaller than the internal length λ of the stress-driven nonlocal model, nonlocal effects become more significant in the travelling waves. Focusing on each branch, comments on its variation with λ are consistent with those made for the bare microbeam in Fig. 4: (i) for fixed wave number q, the frequency ω increases with λ, confirming the stiffening effects for increasing λ; (ii) for fixed frequency ω, the deviation of the nonlocal response from the local one is more significant for increasing λ, as expected since λ governs the length of the beam domain where nonlocal effects are relevant.

Fig. 6 reports the $q(\omega)$ dispersion curves obtained by solving the eigenvalue problem in Eq. (39) with $M = 2$, retaining, in agreement with similar studies (Xiao et al., 2012), the essential information on wave dispersion, i.e., the purely real wave numbers q (the positive ones only, for conciseness) and the absolute values of the imaginary parts of complex-valued or purely imaginary wave numbers q; indeed, the first describe the propagating waves, the second indicate the attenuation at every frequency ω. The results in Fig. 6 agree with those in Fig. 5: indeed, both band gaps are identical to those shown in Fig. 5 and,

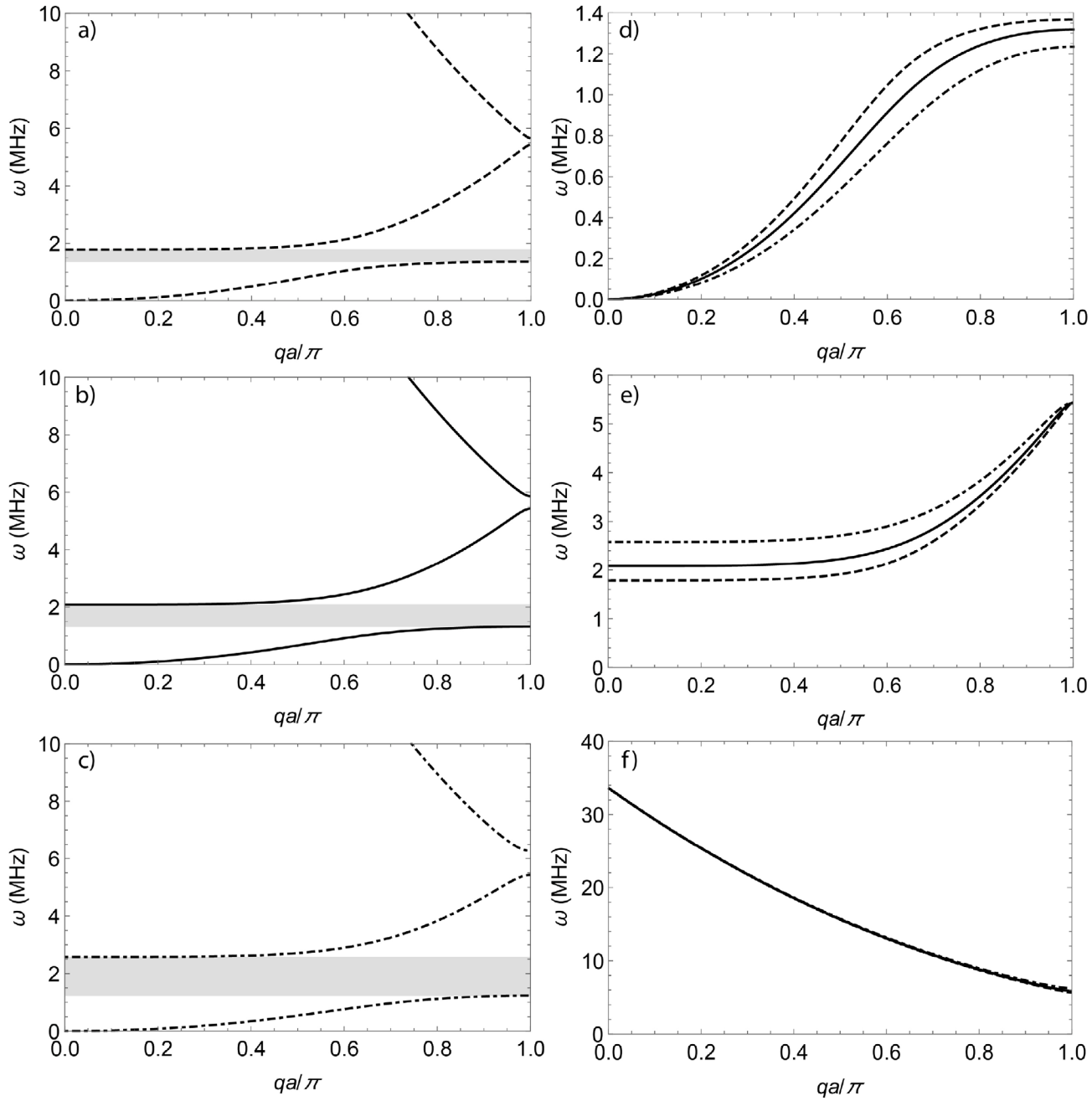

Fig. 9. $\omega(q)$ dispersion curves of periodic stress-driven nonlocal Timoshenko microbeam with mass-spring resonators for $\lambda = 30$ μm and different mass ratios $m_r/\rho Aa$, $m_r/\rho Aa = 0.58$ thick dashed line, $m_r/\rho Aa = 1.16$ thick continuous line, $m_r/\rho Aa = 2.32$ thick dot-dashed line; first three branches for separate values of $m_r/\rho Aa$ (left column): (a) $m_r/\rho Aa = 0.58$, (b) $m_r/\rho Aa = 1.16$, (c) $m_r/\rho Aa = 2.32$; single branches for all considered values of $m_r/\rho Aa$ (right column): (d) first branch, (e) second branch, (f) third branch; grey bands indicate local resonance band gaps.

for fixed frequency ω, the deviation of the nonlocal response from the local one is more significant for increasing λ (see, in particular, the real branches). Additional comments are in order on the attenuation. It is observed that the attenuation is affected by λ over the whole frequency range, including the local resonance band gap. In general, the attenuation reduces with increasing λ and the reduction becomes more evident in the high frequency range. The zoomed view of the imaginary part within the Bragg band gap, shown in Fig. 6, demonstrates that the attenuation within the Bragg band gap is generally very low and decreases for increasing λ. Consistently with Fig. 5, Fig. 6 confirms that the opening frequency of the Bragg band gap shifts to higher frequencies for increasing λ and, moreover, that the size of the Bragg band gap reduces for increasing λ.

To validate the band structure obtained for the infinite beam, consider a finite periodic stress-driven nonlocal Timoshenko microbeam with mass-spring resonators, as shown in Fig. 7. It consists of 10 cells (total length of the microbeam equal to $10a$) and is acted upon by a unit harmonic deflection at the left end; its transmittance, obtained as ratio of the deflection at the right end to the (unit) deflection at the left end, is reported in Fig. 8. Fig. 8 shows that the transmittance attains very low values within the local resonance band gap predicted by the wave propagation analysis of the infinite beam, reported in Figs. 5 and 6. On the other hand, no significantly low values of the transmittance are observed in the Bragg band gap predicted by the wave propagation analysis of the infinite beam, in agreement with the very low attenuation found within the Bragg band gap in Fig. 6. These

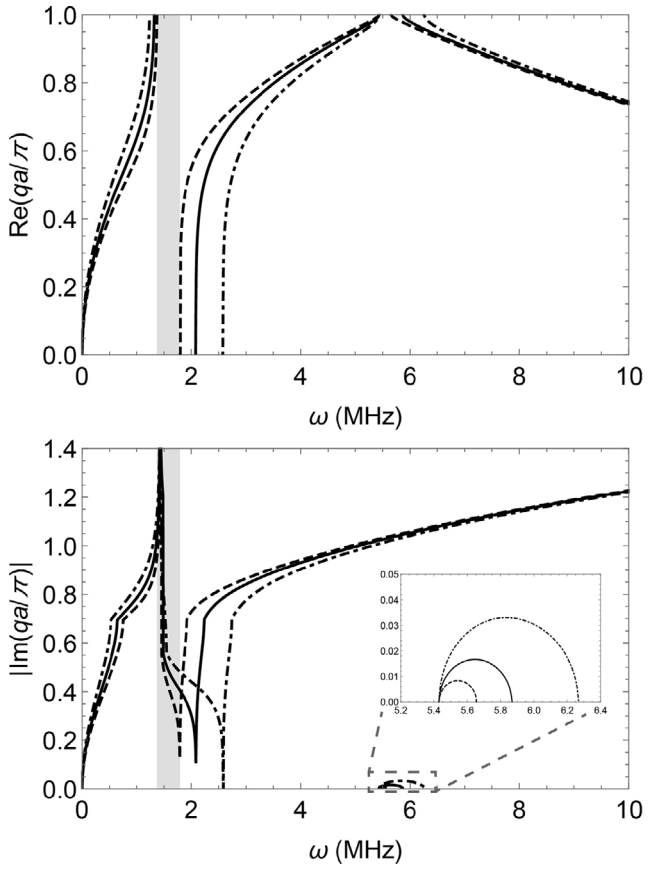

Fig. 10. $q(\omega)$ dispersion curves of periodic stress-driven nonlocal Timoshenko microbeam with mass-spring resonators for $\lambda = 30$ μm and different mass ratios $m_r/\rho Aa$, $m_r/\rho Aa = 0.58$ thick dashed line, $m_r/\rho Aa = 1.16$ thick continuous line, $m_r/\rho Aa = 2.32$ thick dot-dashed line; real parts (top row) and imaginary parts (bottom row); grey band indicates local resonance band gap for lowest mass ratio $m_r/\rho Aa = 0.58$ among considered ones.

are remarkable results, confirming that wave attenuation properties of the infinite beam hold also for the finite one.

Next, it is of interest to assess whether the band structure is affected by varying the mass ratio $m_r/\rho Aa$, with m_r mass of the resonator and ρAa mass of the cell (ρ denotes the mass density of the material, $A = B \times H$ the area of the cross section, a the length of the cell, see definitions above). For this purpose, increasing values for the mass m_r of the resonator are considered, while keeping ρ, A and a as assumed in Figs. 5, 6, 8. Further, since the effects of varying the mass ratio only are sought, the tuning frequency of the mass-spring resonator is kept unchanged by varying accordingly the stiffness k_r of the resonator; that is, the tuning frequency is always $\omega_r = 1.424$ MHz as assumed in Figs. 5, 6, 8. The results are shown in Figs. 9 and 10 for $m_r/\rho Aa = 0.58, 1.16, 2.32$, assuming the fixed internal length $\lambda = 30$ μm; $m_r/\rho Aa = 1.16$ is the mass ratio used in Figs. 5, 6, 8. Fig. 9 demonstrates that increasing the mass ratio causes the size of the local resonance band gap to increase. Interestingly, a similar behaviour is encountered in the local beam, according to existing literature in the field (Sugino et al., 2017). Fig. 9 also shows that the size of the Bragg band gap increases for increasing mass ratio. Moreover, it is observed that the opening frequency of the local resonance band gap shifts slightly below the tuning frequency of the mass-spring resonators for increasing mass ratio, while the opening frequency of the Bragg band gap is almost unchanged. Changes in the dispersion branches are consistent with the variations of local resonance band gap and Bragg band gap with the mass ratio; in particular, changes are significant in the first two branches. Finally, Fig. 10 shows that the attenuation is affected by the mass ratio and, in particular, that increasing the mass ratio is beneficial to the attenuation within the local resonance band gap and to the attenuation within the Bragg band gap as well. Results for different values of λ mirror those in Figs. 9 and 10 and are not included for brevity.

6.3. Periodic stress-driven nonlocal Timoshenko microbeam on elastic supports

Next, consider an infinite periodic stress-driven nonlocal Timoshenko microbeam on elastic supports, as shown in Fig. 3. It is assumed that the microbeam models a micropipe with the following parameters, taken from Zhao et al. (2018): $a = 170$ μm, $R_o = 10$ μm (outer radius), $R_i = 0.9R_o$ (inner radius), $E = 70$ GPa, $G = 26.3$ GPa and $\rho = 2700$ kg/m^3. In particular, it is of interest to investigate the wave dispersion properties for stiff supports, here modelled assuming $k_s = 10^{13} \times GA_s/a = 4.62 \times 10^{16}$ N/m, i.e., a large multiplier of the shear stiffness of the microbeam. To analyse the influence of nonlocal effects, $\lambda = 0$ μm (local Timoshenko beam), $\lambda = 64$ μm, $\lambda = 128$ μm and $\lambda = 192$ μm are selected for the internal length λ; for the selected $a = 170$ μm, they correspond to $\lambda/a = 0.376, 0.753, 1.129$, i.e., almost the same ratios λ/a used in Section 6.2.

Fig. 11 shows the first five dispersion branches calculated by solving the eigenvalue problem in Eq. (40) with $M = 3$. No eigenvalues are found in separate Bragg band gaps, where no waves can propagate. The opening frequencies of the Bragg band gaps shift to higher frequencies and their sizes increase for increasing λ; three Bragg band gaps are found for $\lambda = 64$ μm and two Bragg band gaps for $\lambda = 128$ μm and $\lambda = 192$ μm in the considered frequency range. As for the dispersion curves, it is seen that, for any λ, each nonlocal branch deviates from the corresponding local branch, with more evident deviations in the higher frequency branches. Again, this result confirms that nonlocal effects play a major role at higher frequencies, as observed for the periodic microbeam with mass-spring-resonators in Fig. 5 and Fig. 6 and the bare microbeam in Fig. 4. Fig. 11 also shows that nonlocal effects in the higher frequency range make the shape of some nonlocal branches rather different from the shape of the corresponding local ones. Focusing the attention on how each branch varies with λ, it is observed that, for fixed wave number q, the frequency ω increases with λ, confirming the stiffening effects for increasing λ observed for the bare microbeam in Fig. 4.

Fig. 12 depicts the $q(\omega)$ dispersion curves obtained by solving the eigenvalue problem in Eq. (39) with $M = 3$ and, in particular, the purely real wave numbers q and the absolute values of the imaginary parts of complex-valued or purely imaginary wave numbers q. The Bragg band gaps are identical to those shown in Fig. 11. As for the attenuation within the band gaps, it is observed that it slightly decreases in the first Bragg band gap for increasing λ, while it is almost unchanged in the others. In agreement with Fig. 11, Fig. 12 shows that the opening frequencies of the Bragg band gaps shift to higher frequencies and their sizes increase for increasing λ.

Next, the transmittance of a finite periodic stress-driven nonlocal Timoshenko microbeam on elastic supports is calculated to validate the band structure obtained for the infinite one. To this aim, the finite microbeam in Fig. 13 is considered, including 10 cells (total length of the microbeam equal to $10a$) and subjected to a unit deflection at the left end. Fig. 14 shows that its transmittance, calculated as ratio of the deflection at the right end to the (unit) deflection at the left end, attains very low values within the band gaps predicted by the wave propagation analysis, confirming once again that the attenuation properties of the infinite beam hold for the finite beam as well.

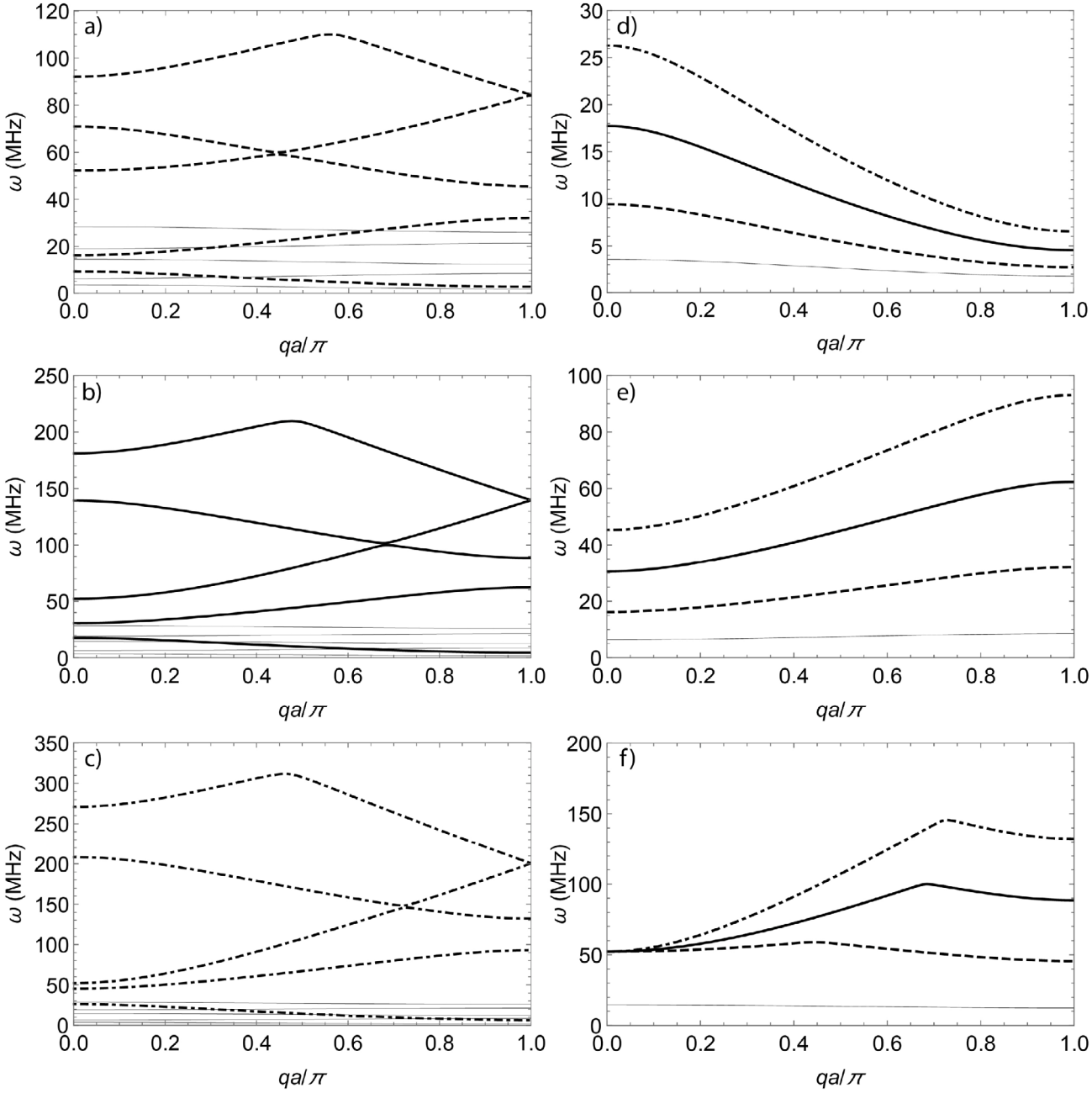

Fig. 11. $\omega(q)$ dispersion curves of stress-driven nonlocal Timoshenko microbeam on elastic supports for different internal lengths λ, $\lambda = 0$ (local) thin continuous line, $\lambda = 64$ μm thick dashed line, $\lambda = 128$ μm thick continuous line, $\lambda = 192$ μm thick dot-dashed line; first five branches for separate values of λ (left column): (a) $\lambda = 0$ and $\lambda = 64$ μm, (b) $\lambda = 0$ and $\lambda = 128$ μm, (c) $\lambda = 0$ and $\lambda = 192$ μm; single branches for all considered values of λ (right column): (d) first branch, (e) second branch, (f) third branch.

6.4. Size effects in periodic stress-driven nonlocal Timoshenko microbeam on elastic supports

Finally, it is of interest to assess whether the stress-driven nonlocal Timoshenko beam model is capable of capturing size effects, as the size of the beam reduces. To this aim, building on the example in Section 6.3, the band structure calculated for a stress-driven nonlocal Timoshenko microbeam on elastic supports is compared with the corresponding one calculated by the classical local Timoshenko beam model, assuming that the outer radius R_o of the cross section and the mutual distance a of the supports decrease while the ratio R_o/a^2 is kept constant. Indeed, numerical evidence shows that the Timoshenko local beam theory does not predict appreciable changes in the band structure of the microbeam, if R_o and a change with $R_o/a^2 = const$. Specifically, Fig. 15 shows the $\omega(q)$ dispersion curves of a microbeam for three decreasing values for the outer radius of the cross section, i.e., $R_o = 2$ μm, $R_o = 1$ μm, $R_o = 0.5$ μm, with $R_o/a^2 = const$ (the corresponding mutual distances a of the supports are $a = 424$ μm, $a = 300$ μm, $a = 212$ μm) and internal length $\lambda = 342$ μm for the stress-driven nonlocal model. The stiffness of the supports is $k_s = 10^9 \times GA_s/a$, while the other parameters of the microbeam are the same as in Section 6.3. It is observed that the classical local Timoshenko beam model predicts the same band structure for any outer radius R_o of the cross section. On the contrary, the stress-driven nonlocal Timoshenko beam model predicts stiffening size effects, as the dispersion curves and the opening frequencies of the Bragg band gaps shift to higher frequencies as R_o reduces. It is worthwhile remarking that stiffening size effects in beam-like structures at the microscale are well documented in the literature (Lam et al.,

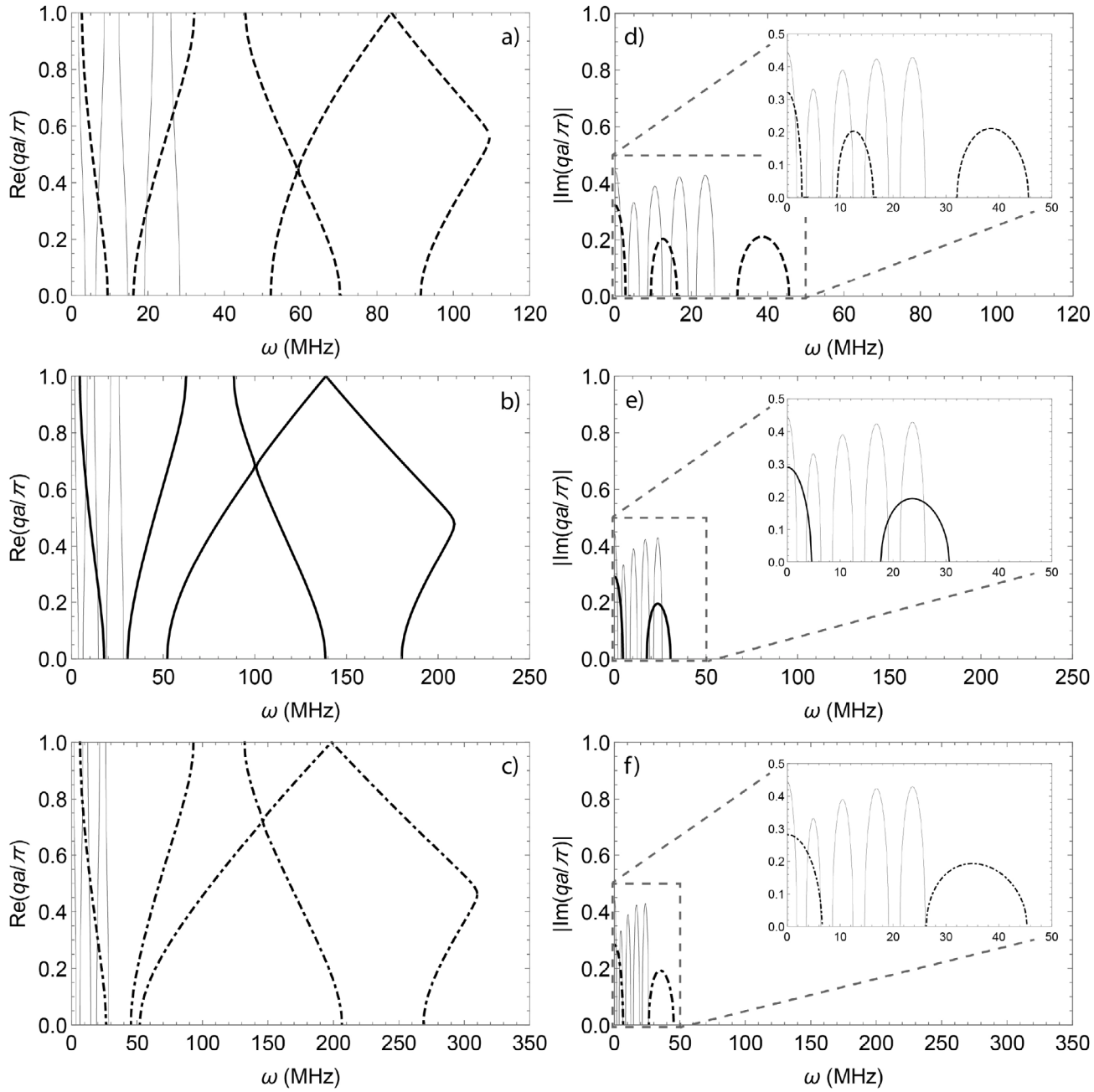

Fig. 12. $q(\omega)$ dispersion curves of stress-driven nonlocal Timoshenko microbeam on elastic supports for different internal lengths λ, $\lambda = 0$ (local) thin continuous line, $\lambda = 64$ μm thick dashed line, $\lambda = 128$ μm thick continuous line, $\lambda = 192$ μm thick dot-dashed line; real parts (left column) and imaginary parts (right column) for separate values of λ: (a,d) $\lambda = 0$ and $\lambda = 64$ μm, (b,e) $\lambda = 0$ and $\lambda = 128$ μm, (c,f) $\lambda = 0$ and $\lambda = 192$ μm.

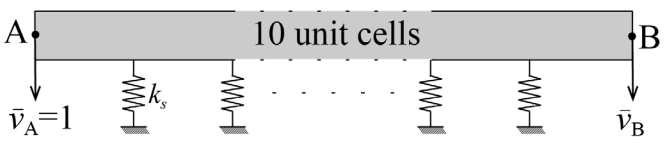

Fig. 13. Finite periodic stress-driven nonlocal Timoshenko microbeam on elastic supports.

2003; McFarl and Colton, 2005; Lei et al., 2016; Li et al., 2018, 2019; Choi et al., 2022), for decreasing size of the specimens.

7. Conclusion

This work has dealt with wave propagation in small-size beams, proposing a stress-driven nonlocal Timoshenko beam formulation and developing an original analytical/computational framework for bare and periodic beams. Infinite and finite beams have been addressed, introducing the following relevant novelties: (i) exact analytical expressions of the dispersion curves for the bare beam, providing full insight into the effects of nonlocality; (ii) an exact PWE method for periodic beams either equipped with mass-spring resonators or resting on elastic supports, delivering both $\omega(q)$ and $q(\omega)$ dispersion curves; (iii) an approximate homogenization approach for periodic beams, estimating opening frequencies and sizes of band gaps induced by mass-spring resonators; (iv) a two-field finite element method to calculate

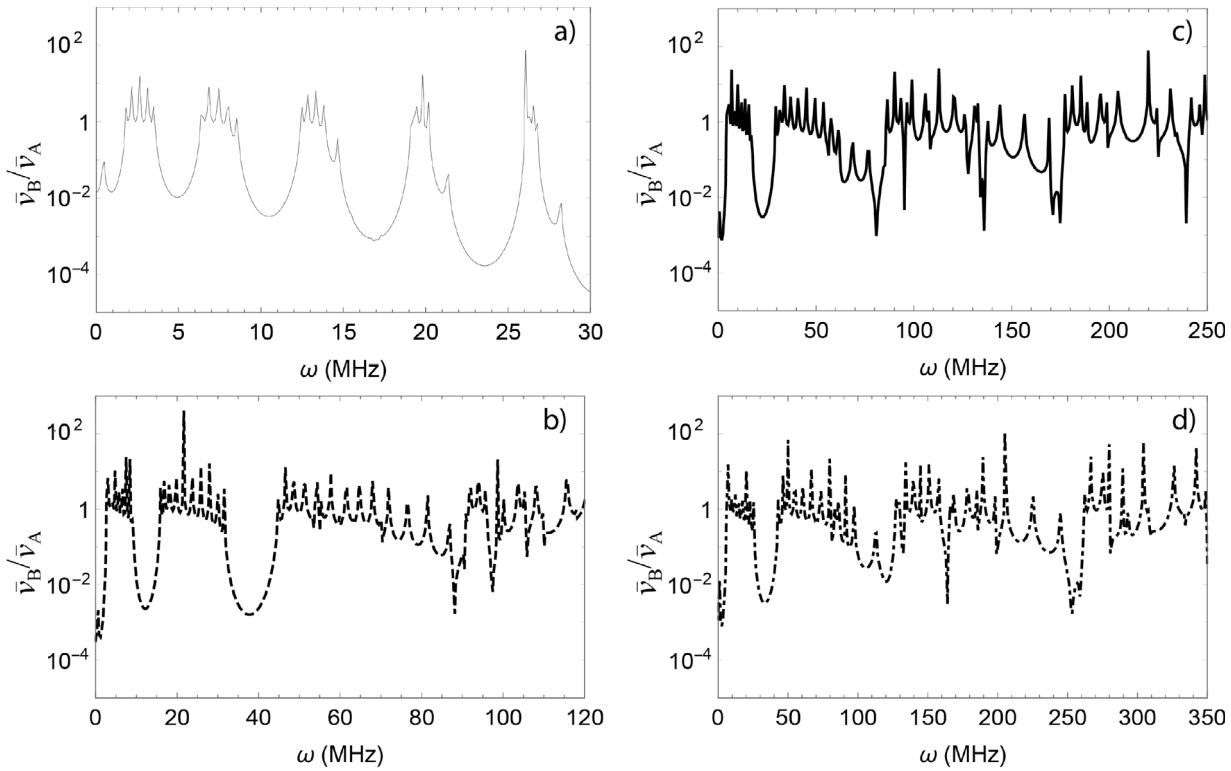

Fig. 14. Transmittance of finite periodic stress-driven nonlocal Timoshenko microbeam on elastic supports in Fig. 13 for different internal lengths λ: (a) $\lambda = 0$ (local) thin continuous line, (b) $\lambda = 64$ μm thick dashed line, (c) $\lambda = 128$ μm thick continuous line, (d) $\lambda = 192$ μm thick dot-dashed line.

the transmittance of finite periodic beams, involving displacements and stresses as well. The stress-driven nonlocal model features an integral formulation and an equivalent differential one: the differential formulation has been used to build wave solutions/methods for infinite beams (i.e., dispersion curves of bare beam, PWE method and homogenization approach for periodic beams), the integral formulation to construct the two-field finite element method for finite periodic beams. Numerical applications have investigated the dispersion diagram of bare and periodic beams for different internal lengths of the stress-driven nonlocal model. Predictions from wave propagation analysis have been validated by transmittance of finite periodic beams. This is an important conclusion of this work, demonstrating not only the correctness of the proposed PWE method, homogenization approach and two-field finite element method but also the theoretical consistency between the differential formulation of the stress-driven nonlocal model used for infinite beams and its integral formulation used for finite ones. Other important conclusions drawn in this study are that the stress-driven nonlocal Timoshenko beam model is stiffer than the classical local Timoshenko one and predicts stiffening size effects with reducing size of the beam; stiffening size effects are in agreement with numerical and experimental evidence on microbeams.

CRediT authorship contribution statement

Gioacchino Alotta: Writing - review & editing, Writing - original draft, Visualization, Validation, Software, Methodology, Conceptualization. **Andrea Francesco Russillo:** Validation, Software, Methodology, Conceptualization. **Giuseppe Failla:** Writing - review & editing, Writing - original draft, Supervision, Methodology, Funding acquisition, Conceptualization.

Declaration of competing interest

The authors declare that they have no known competing financial interests or personal relationships that could have appeared to influence the work reported in this paper.

Acknowledgements

The authors gratefully acknowledge the financial support of the Italian Ministry of University and Research (MUR), PRIN 2022: “Innovative Metamaterial Components and Absorbers for Vibration Mitigation (METAVIBRA)”, grant number: 2022LA43E2.

Appendix A. Homogenization approach

This Appendix presents a homogenization approach for periodic stress-driven nonlocal Timoshenko beam with mass-spring resonators.

It is known that homogenization methods are meaningful for wave propagation analysis as long as the length of the unit cell, i.e., the distance between consecutive resonators is small compared to the wavelength of the travelling wave. Under this assumption, the reaction force of each resonator on the beam can be reverted to a distributed force per unit length along the unit cell. It follows that Eqs. (17) are rewritten as

$$-\left[\left(v^{(2)}(x,t)+\varphi^{(1)}(x,t)\right)-\lambda^2\left(v^{(4)}(x,t)+\varphi^{(3)}(x,t)\right)\right]+ \\ +\alpha\ddot{v}(x,t)=\overline{\kappa}_r\left(w(x,t)-v(x,t)\right) \tag{A.1a}$$

$$-\left(\varphi^{(2)}(x,t)-\lambda^2\varphi^{(4)}(x,t)\right)+\beta\left[\left(v^{(1)}(x,t)+\varphi(x,t)\right)\right. \\ \left.-\lambda^2\left(v^{(3)}(x,t)+\varphi^{(2)}(x,t)\right)\right]+\eta\ddot{\varphi}(x,t)=0 \tag{A.1b}$$

$$-k_r\left(v(x,t)-w(x,t)\right)+m_r\ddot{w}_j(t)=0 \tag{A.1c}$$

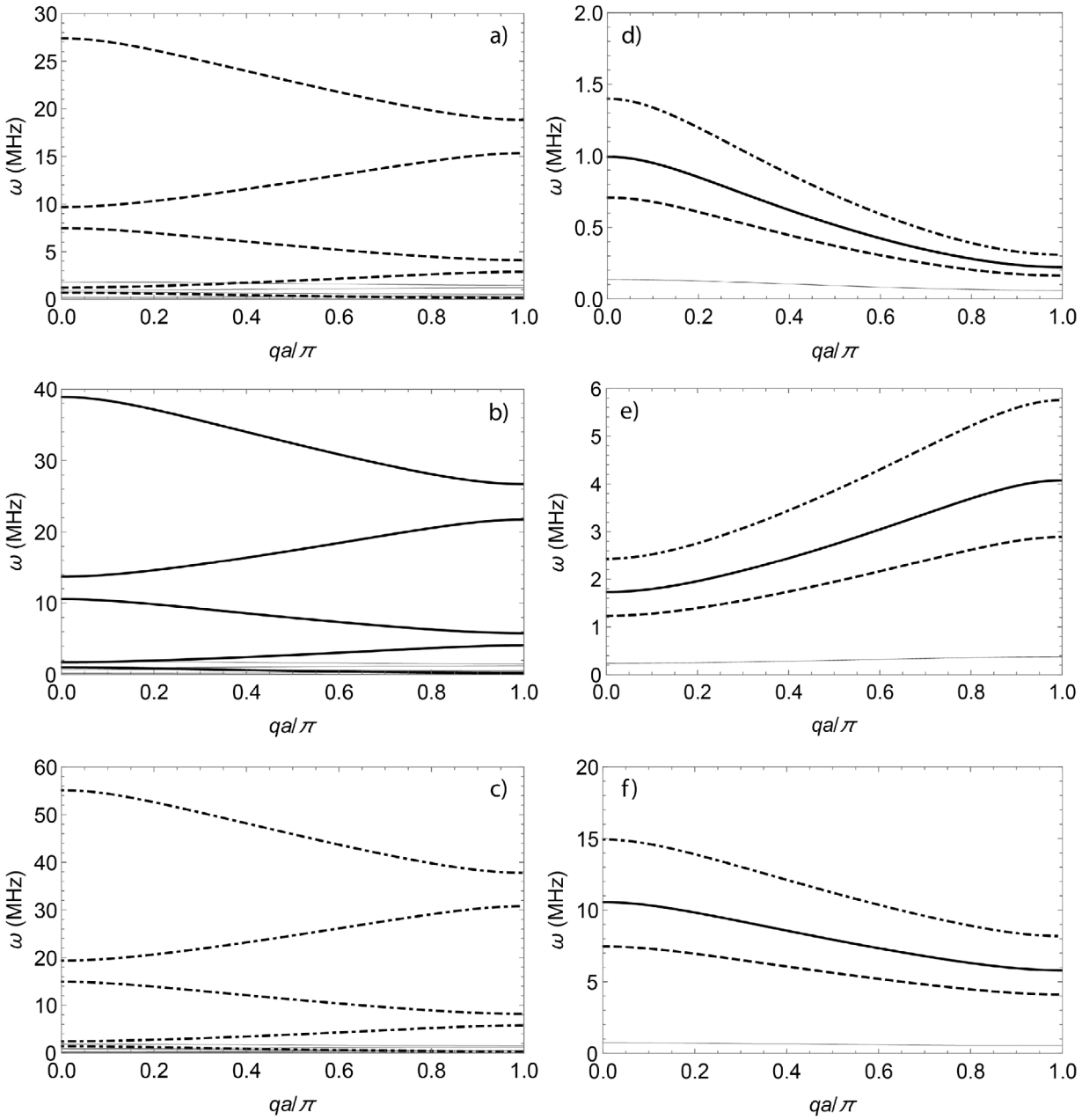

Fig. 15. $\omega(q)$ dispersion curves of periodic stress-driven nonlocal Timoshenko microbeam on elastic supports for different outer radii R_o of the cross section with $R_o/a^2 = const$, $R_o = 2$ μm, $R_o = 1$ μm, $R_o = 0.5$ μm, internal lengths $\lambda = 0$ (local) thin continuous line and $\lambda = 342$ μm ($R_o = 2$ μm thick dashed line, $R_o = 1$ μm thick continuous line, $R_o = 0.5$μm thick dot-dashed line); first five branches for separate values of outer radius R_o (left column): (a) $R_o = 2$ μm, (b) $R_o = 1$ μm, (c) $R_o = 0.5$ μm; single branches for all outer radii R_o (right column): (d) first branch, (e) second branch, (f) third branch.

The system in Eq. (A.1) is solved with the same procedure developed in Section 3, hence Eqs. (9) and $w(x,t) = w_0 e^{i(\omega t+qx)}$ are used into Eqs. (A.1), yielding

$$\left[q^2\left(1+\lambda^2q^2\right)-\alpha\omega^2\right]v_0 - iq\left(1+\lambda^2q^2\right)\varphi_0 - \overline{\kappa}_r(w_0-v_0) = 0 \tag{A.2a}$$

$$i\beta q\left(1+\lambda^2q^2\right)v_0 + \left[\left(q^2+\beta\right)\left(1+\lambda^2q^2\right)-\eta\omega^2\right]\varphi_0 = 0 \tag{A.2b}$$

$$-k_r\left(v_0-w_0\right) - m_r\omega^2 w_0 = 0 \tag{A.2c}$$

The system in Eq. (A.2) is recast in compact form as

$$\mathbf{B}\mathbf{d}_0^* = \mathbf{0} \tag{A.3}$$

where $\mathbf{d}_0^* = [v_0\ \varphi_0\ w_0]^T$ and

$$\mathbf{B} = \begin{bmatrix} q^2\left(1+\lambda^2q^2\right)-\alpha\omega^2+\overline{\kappa}_r & -iq\left(1+\lambda^2q^2\right) & -\overline{\kappa}_r \\ i\beta q\left(1+\lambda^2q^2\right) & \left(q^2+\beta\right)\left(1+\lambda^2q^2\right)-\eta\omega^2 & 0 \\ -k_r & 0 & \left(k_r-m_r\omega^2\right) \end{bmatrix} \tag{A.4}$$

The solutions $\omega(q)$ are found from the following equation obtained by setting $\det\mathbf{B} = 0$:

$$b_6\omega^6 + b_4\omega^4 + b_2\omega^2 + b_0 = 0 \tag{A.5a}$$

$$b_6 = -\alpha\eta = -a_4 \tag{A.5b}$$

$$b_4 = \left[\alpha\beta + q^2(\alpha+\eta)\right]\left(1+\lambda^2q^2\right) + \eta\left(\overline{\kappa}_r + \alpha\omega_r^2\right) = -a_2 + \eta\left(\overline{\kappa}_r + \alpha\omega_r^2\right) \tag{A.5c}$$

$$b_2 = -\left\{\lambda^2 q^6 + q^4 + \left[\overline{\kappa}_r + (\alpha+\eta)\,\omega_r^2\right] q^2 + \beta\left(\overline{\kappa}_r + \alpha\omega_r^2\right)\right\}\left(1+\lambda^2 q^2\right) \tag{A.5d}$$

$$b_0 = q^4\left(1+\lambda^2 q^2\right)^2 \omega_r^2 = a_0\omega_r^2 \tag{A.5e}$$

where $\omega_r^2 = k_r/m_r$. Eq. (A.5) has six solutions $\omega(q)$ that can be written as follows

$$\omega_{1,2}(q) = \pm\frac{1}{\sqrt{6b_6}}\sqrt{2^{2/3}d_1 - 2b_4 + 2^{4/3}\frac{d_2}{d_1}} \tag{A.6a}$$

$$\omega_{3,4}(q) = \pm\frac{1}{2\sqrt{3b_6}}\sqrt{-2^{2/3}d_1\left(1+i\sqrt{3}\right) - 4b_4 - 2^{4/3}\left(1-i\sqrt{3}\right)\frac{d_2}{d_1}} \tag{A.6b}$$

$$\omega_{5,6}(q) = \pm\frac{1}{2\sqrt{3b_6}}\sqrt{-2^{2/3}d_1\left(1-i\sqrt{3}\right) - 4b_4 - 2^{4/3}\left(1+i\sqrt{3}\right)\frac{d_2}{d_1}} \tag{A.6c}$$

where

$$d_1 = \left(d_3 + \sqrt{d_3^2 - 4d_2^3}\right)^{1/3} \tag{A.7a}$$

$$d_2 = b_4^2 - 3b_2b_6 \tag{A.7b}$$

$$d_3 = 9b_2b_4b_6 - 27b_0a_6^2 - 2b_4^3 \tag{A.7c}$$

In agreement with other applications of homogenization methods in the literature, in this work the homogenization approach proves useful to estimate approximately opening frequencies and sizes of band gaps associated with local resonance, as shown in Section 6. However, the effect of periodicity is not explicitly taken into account, as indeed the dispersion equation is not obtained by enforcing the Bloch condition relating the responses over two adjacent cells (Liu et al., 2007). Therefore, the homogenization approach cannot capture Bragg effects and related band gaps, which is a known limitation of homogenization methods pointed out in previous studies, e.g., see Thai et al. (2017), Barretta et al. (2024), Sugino et al. (2017).

Appendix B. Transmittance of finite periodic stress-driven nonlocal Timoshenko beam

This Appendix formulates a two-field finite element method, which involves displacements and stresses as primary variables, to calculate the transmittance of finite periodic stress-driven nonlocal Timoshenko beams. The method relies on the integral formulation (2) of the constitutive laws and differs, in this respect, from the methods developed in Section 3 through Section 5, where the differential Eqs. (4) are used for shear force and bending moment. The transmittance, calculated from the frequency response of the beam, is of particular interest to assess whether the dispersion properties calculated for infinite beams in Sections 4 and 5 hold for finite beams as well. The method is inspired by the two-field finite element formulation in the textbook (Zienkiewicz et al., 2005); a two-field finite element method for stress-driven nonlocal 3D solids was proposed by some of the authors in Russillo et al. (2022).

It is assumed that the finite beam consists of a number of cells N. Be the beam response at the steady state under a harmonic excitation with frequency ω. Assuming the solution of Eqs. (4)-(6) in the form

$$\begin{aligned}
&\gamma(x,t) = \overline{\gamma}(x)\mathrm{e}^{\mathrm{i}\omega t}\\
&\chi(x,t) = \overline{\chi}(x)\mathrm{e}^{\mathrm{i}\omega t}\\
&T(x,t) = \overline{T}(x)\mathrm{e}^{\mathrm{i}\omega t}\\
&M(x,t) = \overline{M}(x)\mathrm{e}^{\mathrm{i}\omega t}
\end{aligned} \tag{B.1}$$

leads to the following integro-differential system of equations:

$$\begin{cases}
\overline{T}^{(1)}(x) + \rho A\omega^2\overline{v}(x) = 0\\
\overline{M}^{(1)}(x) - \overline{T}(x) + \rho I_y\omega^2\overline{\varphi}(x) = 0\\
\overline{\gamma}(x) = \dfrac{1}{GA_s}\displaystyle\int_a^b \boldsymbol{\Phi}(x,\xi)\overline{T}(\xi)\,\mathrm{d}\xi\\
\overline{\chi}(x) = \dfrac{1}{EI_y}\displaystyle\int_a^b \boldsymbol{\Phi}(x,\xi)\overline{M}(\xi)\,\mathrm{d}\xi
\end{cases} \tag{B.2}$$

Next, on partitioning the beam domain in n finite elements, i.e., $[a,b] = [a_1,a_2]\cup[a_2,a_3]\cup\cdots\cup[a_n,b_n]$, the principle of virtual work gives the following weak formulation over each subdomain $[a_k,b_k]$ $(k=1,\ldots,n)$:

$$\begin{cases}
\displaystyle\int_{a_k}^{b_k}\overline{T}(x)\delta\overline{\gamma}(x)\,\mathrm{d}x + \int_{a_k}^{b_k}\overline{M}(x)\delta\overline{\chi}(x)\,\mathrm{d}x - \rho A\omega^2\int_{a_k}^{b_k}\overline{v}(x)\delta\overline{v}(x)\mathrm{d}x\\
\displaystyle -\rho I_y\omega^2\int_{a_k}^{b_k}\overline{\varphi}(x)\delta\overline{\varphi}(x)\mathrm{d}x = \overline{T}_k\delta\overline{\gamma}_k + \overline{T}_{k+1}\delta\overline{\gamma}_{k+1} + \overline{M}_k\delta\overline{\chi}_k + \overline{M}_{k+1}\delta\overline{\chi}_{k+1}\\
\displaystyle\int_{a_k}^{b_k}\overline{\gamma}(x)\delta\overline{T}(x)\,\mathrm{d}x + \int_{a_k}^{b_k}\overline{\chi}(x)\delta\overline{M}(x)\,\mathrm{d}x - \frac{1}{GA_s}\int_{a_k}^{b_k}\int_a^b \boldsymbol{\Phi}(x,\xi)\overline{T}(\xi)\delta\overline{T}(x)\,\mathrm{d}\xi\,\mathrm{d}x\\
\displaystyle -\frac{1}{EI_y}\int_{a_k}^{b_k}\int_a^b \boldsymbol{\Phi}(x,\xi)\overline{M}(\xi)\delta\overline{M}(x)\,\mathrm{d}\xi\,\mathrm{d}x = 0
\end{cases} \tag{B.3}$$

Making use of the kinematic compatibility equations (1) and assuming the isoparametric expansions for the primary variables

$$\overline{w}_k(x) = \mathbf{N}_w(x)\overline{\mathbf{w}}_k; \quad \overline{s}_k(x) = \mathbf{N}_s(x)\overline{\mathbf{s}}_k \tag{B.4}$$

where $\overline{\mathbf{w}}_k = \begin{bmatrix}\overline{\mathbf{v}}_k^{\mathrm{T}} & \overline{\boldsymbol{\varphi}}_k^{\mathrm{T}}\end{bmatrix}^{\mathrm{T}}$ and $\overline{\mathbf{s}}_k = \begin{bmatrix}\overline{\mathbf{T}}_k^{\mathrm{T}} & \overline{\mathbf{M}}_k^{\mathrm{T}}\end{bmatrix}^{\mathrm{T}}$ are the vectors collecting the nodal generalized displacements and forces at the nodes of the kth element, $\mathbf{N}_w$ and $\mathbf{N}_s$ are the corresponding linear shape function matrices, the following equation is obtained for the kth element:

$$\left(\begin{bmatrix}\mathbf{0} & \mathbf{B}_k\\ \mathbf{B}_k^{\mathrm{T}} & -\mathbf{C}_k\end{bmatrix} - \omega^2\begin{bmatrix}\mathbf{M}_k & \mathbf{0}\\ \mathbf{0} & \mathbf{0}\end{bmatrix}\right)\begin{bmatrix}\overline{\mathbf{w}}_k\\ \overline{\mathbf{s}}_k\end{bmatrix} = \begin{bmatrix}\overline{\mathbf{f}}_k\\ \mathbf{0}\end{bmatrix} \tag{B.5}$$

Eq. (B.5) is the two-field finite element equation governing the steady state response of the kth element, where vector $\overline{\mathbf{f}}_k$ collects the external nodal forces. The corresponding equation for the whole beam coupled with either mass-spring resonators or elastic supports can be obtained by an assembling procedure enforcing continuity of displacements and forces at all nodes, except for the shear forces at the nodes where mass-spring resonators/elastic supports are located. This leads to the following equation for the whole beam:

$$\left(\begin{bmatrix}\mathbf{0} & \mathbf{B}\\ \mathbf{B}^{\mathrm{T}} & -\mathbf{C}\end{bmatrix} - \omega^2\begin{bmatrix}\mathbf{M} & \mathbf{0}\\ \mathbf{0} & \mathbf{0}\end{bmatrix}\right)\begin{bmatrix}\overline{\mathbf{w}}\\ \overline{\mathbf{s}}\end{bmatrix} = \begin{bmatrix}\overline{\mathbf{f}}\\ \mathbf{0}\end{bmatrix} \tag{B.6}$$

where $\overline{\mathbf{w}} = \begin{bmatrix}\overline{\mathbf{v}}^{\mathrm{T}} & \overline{\boldsymbol{\varphi}}^{\mathrm{T}}\end{bmatrix}^{\mathrm{T}}$ and $\overline{\mathbf{s}} = \begin{bmatrix}\overline{\mathbf{T}}^{\mathrm{T}} & \overline{\mathbf{M}}^{\mathrm{T}}\end{bmatrix}^{\mathrm{T}}$ are the vectors collecting the nodal generalized displacements and forces at all nodes, $\overline{\mathbf{f}}$ is the vector of external nodal forces, i.e., the vector including the reaction forces of the mass-spring resonators/elastic supports, the reaction forces of any other external constraint on the beam and any external load. Since no continuity of the shear forces is enforced at the nodes where mass-spring resonators/elastic supports are located, vector $\overline{\mathbf{s}}$ in Eq. (B.6) includes two unknowns at each of these nodes, i.e., the shear forces to the left and right of each of these nodes.

Eq. (B.6) can be used to calculate the transmittance of the beam under harmonic excitations, which may be external loads or displacements at the boundaries of the beam.

Data availability

Data will be made available on request.

References

Aifantis, E., 1999. Gradient deformation models at nano, micro, and macro scales. J. Eng. Mater.-T ASME 121 (2), 189–202.

Aifantis, E.C., 2003. Update on a class of gradient theories. Mech. Mater. 35 (3–6), 259–280.
Aifantis, E.C., 2009. Exploring the applicability of gradient elasticity to certain micro/nano reliability problems. Microsyst. Technol. 15 (1), 109–115.
Aifantis, E.C., 2011. On the gradient approach-relation to Eringen's nonlocal theory. Int. J. Eng. Sci. 49 (12), 1367–1377.
Akgöz, B., Civalek, O., 2014. Longitudinal vibration analysis for microbars based on strain gradient elasticity theory. J. Vib. Control 20 (4), 606–616.
Allegri, G., Scarpa, F., Chowdhury, R., Adhikari, S., 2013. Wave propagation in periodically supported nanoribbons: A nonlocal elasticity approach. J. Vib. Acoust. 135, 041017-1.
Alotta, G., Di Paola, M., Failla, G., Pinnola, F.P., 2018. On the dynamics of non-local fractional viscoelastic beams under stochastic agencies. Compos. B Eng. 137, 102–110.
Alotta, G., Di Paola, M., Pinnola, F.P., 2022. An unified formulation of strong non-local elasticity with fractional order calculus. Meccanica 57 (4), 793–805.
Alotta, G., Failla, G., Pinnola, F.P., 2017. Stochastic analysis of a nonlocal fractional viscoelastic bar forced by Gaussian white noise. ASCE-ASME J. Risk Unc. Eng. Syst. Part B Mech. Eng. 3 (3), 030904.
Alotta, G., Failla, G., Zingales, M., 2014. Finite element method for a nonlocal Timoshenko beam model. Finite Elem. Anal. Des. 89, 77–92.
Askes, H., Aifantis, E.C., 2009. Gradient elasticity and flexural wave dispersion in carbon nanotubes. Phys. Rev. B 80 (19), 195412.
Askes, H., Aifantis, E.C., 2011. Gradient elasticity in statics and dynamics: An overview of formulations, length scale identification procedures, finite element implementations and new results. Int. J. Solids Struct. 48 (13), 1962–1990.
Barretta, R., Fazelzadeh, S.A., Feo, L., Ghavanloo, E., Luciano, R., 2018. Nonlocal inflected nano-beams: A stress-driven approach of bi-Helmholtz type. Compos. Struct. 200, 239–245.
Barretta, R., Iuorio, A., Luciano, R., Vaccaro, M.S., 2024. On wave propagation in nanobeams. Int. J. Eng. Sci. 196, 104014.
Behnam-Rasouli, M.-S., Challamel, N., Karamodin, A., Sani, A.A., 2024. Application of the Green's function method for static analysis of nonlocal stress-driven and strain gradient elastic nanobeams. Int. J. Solids Struct. 295, 112794.
Bian, P.-L., Qing, H., 2021. On bending consistency of Timoshenko beam using differential and integral nonlocal strain gradient models. Z. Angew. Math. Mech. 101, e202000132.
Caporale, A., Darban, H., Luciano, R., 2022. Nonlocal strain and stress gradient elasticity of Timoshenko nano-beams with loading discontinuities. Int. J. Eng. Sci. 173, 103620.
Caporale, A., Luciano, R., Scorza, D., Vantadori, S., 2023. Local-nonlocal stress-driven model for multi-cracked nanobeams. Int. J. Solids Struct. 273, 112230.
Challamel, N., Wang, C., Elishakoff, I., 2016. Nonlocal or gradient elasticity macroscopic models: A question of concentrated or distributed microstructure. Mech. Res. Commun. 71, 25–31.
Chen, A.-L., Wang, Y.-S., 2011. Size-effect on band structures of nanoscale phononic crystals. Physica E 44 (1), 317–321.
Choi, J.-H., Kim, H., Kim, J.-Y., Lim, K.-H., Lee, B.-C., Sim, G.-D., 2022. Micro-cantilever bending tests for understanding size effect in gradient elasticity. Mater. Des. 214, 110398.
De Domenico, D., Askes, H., 2018. Stress gradient, strain gradient and inertia gradient beam theories for the simulation of flexural wave dispersion in carbon nanotubes. Compos. B Eng. 153, 285–294.
Demir, C., Civalek, O., 2017. On the analysis of microbeams. Int. J. Eng. Sci. 121, 14–33.
Deng, J., Liu, Y., Liu, W., 2017a. Size-dependent vibration analysis of multi-span functionally graded material micropipes conveying fuid using a hybrid method. Microfluid Nanofluid 21, 133.
Deng, J., Liu, Y., Zhang, Z., Liu, W., 2017b. Size-dependent vibration and stability of multi-span viscoelastic functionally graded material nanopipes conveying fluid using a hybrid method. Compos. Struct. 179, 590–600.
Di Paola, M., Failla, G., Zingales, M., 2009. Physically-based approach to the mechanics of strong non-local linear elasticity theory. J. Elasticity 97, 103–130.
Di Paola, M., Failla, G., Zingales, M., 2010. The mechanically-based approach to 3D non-local linear elasticity theory: Long-range central interactions. Int. J. Solids Struct. 47 (18–19), 2347–2358.
Di Paola, M., Failla, G., Zingales, M., 2013. Non-local stiffness and damping models for shear-deformable beams. Eur. J. Mech. A Solids 40, 69–83.
Ducceschi, M., Bilbao, S., 2019. Conservative finite difference time domain schemes for the prestressed Timoshenko, shear and Euler-Bernoulli beam equations. Wave Motion 89, 142–165.
Ebrahimi, F., Seyfi, A., Dabbagh, A., 2019. A novel porosity-dependent homogenization procedure for wave dispersion in nonlocal strain gradient inhomogeneous nanobeams. Eur. Phys. J. Plus 134, 226.
Eltaher, M.A., Khater, M.E., Emam, S.A., 2016. A review on nonlocal elastic models for bending, buckling, vibrations, and wave propagation of nanoscale beams. Appl. Math. Model. 40 (5–6), 4109–4128.
Eringen, A.C., 1972. Linear theory of nonlocal elasticity and dispersion of plane waves. Int. J. Eng. Sci. 10, 425–435.
Eringen, A.C., 1983. On differential equations of nonlocal elasticity and solutions of screw dislocation and surface waves. J. Appl. Phys. 54 (9), 4703–4710.
Espo, M., Hosseini, S.M., Abolbashari, M.H., 2022. Bandgap characteristics of a piezoelectric phononic crystal Timoshenko nanobeam based on the modified couple stress and surface energy theories. Mater. Today Commun. 33, 104782.
Failla, G., Santini, A., Zingales, M., 2010. Solution strategies for 1D elastic continuum with long-range interactions: Smooth and fractional decay. Mech. Res. Commun. 37 (1), 13–21.
Farajpour, A., Ghayesh, M.H., Farokhi, H., 2018. A review on the mechanics of nanostructures. Int. J. Eng. Sci. 133, 231–263.
Faroughi, S., Rahmani, A., Friswell, M.I., 2020. On wave propagation in two-dimensional functionally graded porous rotating nano-beams using a general nonlocal higher-order beam model. Appl. Math. Model. 80, 169–190.
Ghavanloo, E., Fazelzadeh, S.A., Trovalusci, P., 2023. Mechanics of size-dependent materials. Arch. Appl. Mech. 93, 1–3.
Gomez-Silva, F., Askes, H., 2024. Variationally consistent Elishakoff beam theory: Two finite element implementations and application to flexural wave propagation in carbon nanotubes. J. Sound Vib. 580, 118388.
He, Y., Qing, H., Gao, C.-F., 2020. Theoretical analysis of free vibration of microbeams under different boundary conditions using stress-driven nonlocal integral model. Int. J. Struct. Stab. Dyn. 20 (3), 2050040.
Lakes, R., 1991. Experimental micro mechanics methods for conventional and negative Poisson's ratio cellular solids as cosserat continua. J. Eng. Mater.-T ASME 113 (1), 148–155.
Lam, D.C.C., Yang, F., Chong, A.C.M., Wang, J., Tong, P., 2003. Experiments and theory in strain gradient elasticity. J. Mech. Phys. Solids 51 (8), 1477–1508.
Lei, J., He, Y., Guo, S., Li, Z., Liu, D., 2016. Size-dependent vibration of nickel cantilever microbeams: Experiment and gradient elasticity. AIP Adv. 6 (10), 105202.
Li, Z., He, Y., Lei, J., Guo, S., Liu, D., Wang, L., 2018. A standard experimental method for determining the material length scale based on modified couple stress theory. Int. J. Mech. Sci. 141, 198–205.
Li, Z., He, Y., Lei, J., Han, S., Guo, S., Liu, D., 2019. Experimental investigation on size-dependent higher-mode vibration of cantilever microbeams. Microsyst. Technol. 25, 3005–3015.
Li, C., Qing, H., 2024. Integral nonlocal stress gradient elasticity of functionally graded porous Timoshenko nanobeam with symmetrical or anti-symmetrical condition. Z. Angew. Math. Mech. 104, e202300282.
Lim, C.W., Zhang, G., Reddy, J.N., 2015. A higher-order nonlocal elasticity and strain gradient theory and its applications in wave propagation. J. Mech. Phys. Solids 78, 298–313.
Liu, Y., Yu, D., Zhao, H., Wen, J., Wen, X., 2007. Design guidelines for flexural wave attenuation of slender beams with local resonators. Phys. Lett. A 362, 344–347.
Lu, P., Lee, H.P., Lu, C., Zhang, P.Q., 2007. Application of nonlocal beam models for carbon nanotubes. Int. J. Solids Struct. 44, 5289–5300.
Mancusi, G., Fabbrocino, F., Feo, L., Fraternali, F., 2017. Size effect and dynamic properties of 2D lattice materials. Compos. B Eng. 112, 235–242.
MATLAB R2023b, 2022. Natick. The MathWorks Inc., Massachusetts.
McFarl, A.W., Colton, J.S., 2005. Role of material microstructure in plate stiffness with relevance to microcantilever sensors. J. Micromech. Microeng. 15 (5), 1060–1067.
Mindlin, R.D., 1963. Influence of couple-stresses on stress concentrations. Exp. Mech. 3 (1), 1–7.
Numanoğlu, H.M., Akgöz, B., Civalek, O., 2018. On dynamic analysis of nanorods. Int. J. Eng. Sci. 130, 33–50.
Numanoğlu, H.M., Civalek, O., 2019. On the dynamics of small-sized structures. Int. J. Eng. Sci. 145, 03164.
Patnaik, S., Semperlotti, F., 2020. A generalized fractional-order elastodynamic theory for non-local attenuating media. Proc. R. Soc. Lond. Ser. A Math. Phys. Eng. Sci. 476 (2238), 20200200.
Patnaik, S., Sidhardh, S., Semperlotti, F., 2020. Geometrically nonlinear analysis of nonlocal plates using fractional calculus. Int. J. Mech. Sci. 179, 105710.
Patnaik, S., Sidhardh, S., Semperlotti, F., 2021. Towards a unified approach to nonlocal elasticity via fractional-order mechanics. Int. J. Mech. Sci. 189, 105992.
Polizzotto, C., 2014. Stress gradient versus strain gradient constitutive models within elasticity. Int. J. Solids Struct. 51 (9), 1809–1818.
Polizzotto, C., 2015. A unifying variational framework for stress gradient and strain gradient elasticity theories. Eur. J. Mech. A-Solid 49, 430–440.
Qian, D., 2020. Electro-mechanical coupling wave propagating in a locally resonant piezoelectric/elastic phononic crystal nanobeam with surface effects. Appl. Math. Mech. (English Edition) 41 (3), 425–438.
Qian, D., Wang, J., 2022. Studies of a new-style resonator to control electro-mechanical coupling bandgap of a locally resonant piezoelectric/elastic phononic crystal double-layer nonlocal nanobeam. Appl. Math. Model. 102, 786–796.
Qian, D., Wu, J., He, F., 2021. Electro-mechanical coupling band gaps of a piezoelectric phononic crystal Timoshenko nanobeam with surface effects. Ultrasonics 109, 106225.
Qing, H., Tang, Y., 2023. Size-dependent fracture analysis of centrally-cracked nanobeam using stress-driven two-phase local/nonlocal integral model with discontinuity and symmetrical conditions. Eng. Fract. Mech. 282, 109193.
Romano, G., Barretta, R., 2017a. Nonlocal elasticity in nanobeams: The stress-driven integral model. Int. J. Eng. Sci. 115, 14–27.

Romano, G., Barretta, R., 2017b. Stress-driven versus strain-driven nonlocal integral model for elastic nano-beams. Compos. B Eng. 114, 184–188.
Romano, G., Barretta, R., Diaco, M., 2017a. On nonlocal integral models for elastic nano-beams. Int. J. Mech. Sci. 131–132, 490–499.
Romano, G., Barretta, R., Diaco, M., Marotti de Sciarra, F., 2017b. Constitutive boundary conditions and paradoxes in nonlocal elastic nanobeams. Int. J. Mech. Sci. 121, 151–156.
Roudbari, M.A., Jorshari, T.D., Lü, C., Ansari, R., Kouzani, A.Z., Amabili, M., 2022. A review of size-dependent continuum mechanics models for micro- and nano-structures. Thin Wall. Struct. 170, 108562.
Russillo, A.F., Failla, G., 2022. Wave propagation in stress-driven nonlocal Rayleigh beam lattices. Int. J. Mech. Sci. 215, 106901.
Russillo, A.F., Failla, G., Alotta, G., Marotti de Sciarra, F., Barretta, R., 2021. On the dynamics of nano-frames. Int. J. Eng. Sci. 160, 103433.
Russillo, A.F., Failla, G., Barretta, R., Marotti de Sciarra, F., 2022. On the dynamics of 3D nonlocal solids. Int. J. Eng. Sci. 180, 103742.
Scorza, D., Luciano, R., Vantadori, S., 2022. Fracture behaviour of nanobeams through two-phase local/nonlocal stress-driven model. Comput. Struct. 280, 114957.
Sepehri, S., Jafari, H., Mashhadi, M.M., Yazdi, M.R.H., Fakhrabadi, M.M.S., 2021. Small-scale effects on wave propagation in planar micro-lattices. J. Sound. Vib. 494, 115894.
Sepehri, S., Mashhadi, M.M., Fakhrabadi, M.M.S., 2022. Active/passive tuning of wave propagation in phononic microbeams via piezoelectric patches. Mech. Mater. 167, 104249.
Shaat, M., 2017. A general nonlocal theory and its approximations for slowly varying acoustic waves. Int. J. Mech. Sci. 130, 52–63.
Silling, S.A., 2000. Reformulation of elasticity theory for discontinuities and long-range forces. J. Mech. Phys. Solids 48 (1), 175–209.
Silling, S.A., Epton, M., Weckner, O., Xu, J., Askari, E., 2007. Peridynamic states and constitutive modelings. J. Elasticity 88 (1), 151–184.
Sugino, C., Xia, Y., Leadenham, S., Ruzzene, M., Erturk, A., 2017. A general theory for bandgap estimation in locally resonant metastructures. J. Sound Vib. 406, 104–123.
Tang, Y., Qing, H., 2024. Bi-Helmholtz kernel based stress-driven nonlocal integral model with discontinuity for size-dependent fracture analysis of edge-cracked nanobeam. Mech. Adv. Mater. Struct. 31 (21), 5315–5325.
Thai, H.-T., Vo, T.P., Nguyen, T.-K., Kim, S.-E., 2017. A review of continuum mechanics models for size-dependent analysis of beams and plates. Compos. Struct. 177, 196–219.
Trabelssi, M., El-Borgi, S., Friswell, M.I., 2024. Application of nonlocal strain gradient theory for the analysis of bandgap formation in metamaterial nanobeams. Appl. Math. Model. 127, 281–296.
Wang, L.F., Hu, H.Y., 2005. Flexural wave propagation in single-walled carbon nanotube. Phys. Rev. B 71 (19), 195412-8.
Wang, Q., Liew, K., 2007. Application of nonlocal continuum mechanics to static analysis of micro- and nano-structures. Phys. Lett. A 363 (3), 236–242.
Wang, Q., Shindo, Y., 2006. Nonlocal continuum models for carbon nanotubes subjected to static loading. J. Mech. Mater. Struct. 1 (4), 663–680.
Xiao, Y., Wen, J., Wen, A.X., 2012. Broadband locally resonant beams containing multiple periodic arrays of attached resonators. Phys. Lett. A 376, 1384–1390.
Yan, D.J., Chen, A.-L., Wang, Y.S., Zhang, C., 2020. Size-effect on the band structures of the transverse elastic wave propagating in nanoscale periodic laminates. Int. J. Mech. Sci. 180, 105669.
Yang, F., Chong, A., Lam, D., Tong, P., 2002. Couple stress based strain gradient theory for elasticity. Int. J. Solids Struct. 39 (10), 2731–2743.
Zhang, P., Qing, H., 2021a. Closed-form solution in bi-Helmholtz kernel based two-phase nonlocal integral models for functionally graded Timoshenko beams. Comput. Struct. 265, 113770.
Zhang, P., Qing, H., 2021b. The consistency of the nonlocal strain gradient integral model in size-dependent bending analysis of beam structures. Int. J. Mech. Sci. 189, 105991.
Zhang, P., Qing, H., 2022a. Free vibration analysis of Euler-Bernoulli curved beams using two-phase nonlocal integral models. J. Vib. Control 28 (19–20), 2861–2878.
Zhang, P., Qing, H., 2022b. Well-posed two-phase nonlocal integral models for free vibration of nanobeams in context with higher-order refined shear deformation theory. J. Vib. Control 28 (23–24), 3808–3822.
Zhang, P., Qing, H., 2023. Nonlocal stress gradient integral model with discontinuous and symmetrical conditions for size-dependent fracture of centrally-cracked nanobeams. Mech. Adv. Mater. Struct. 1–12.
Zhang, P., Qing, H., Gao, C.-F., 2020. Analytical solutions of static bending of curved Timoshenko microbeams using Eringen's two-phase local/nonlocal integral model. Z. Angew. Math. Mech. 100, e201900207.
Zhang, P., Schiavone, P., Qing, H., 2022a. Local/nonlocal mixture integral models with bi-Helmholtz kernel for free vibration of Euler-Bernoulli beams under thermal effect. J. Sound Vib. 525, 116798.
Zhang, P., Schiavone, P., Qing, H., 2022b. Stress-driven local/nonlocal mixture model for buckling and free vibration of FG sandwich Timoshenko beams resting on a nonlocal elastic foundation. Comput. Struct. 289, 115473.
Zhao, Y., Deng, J., Liu, Y., Liu, W., 2018. Size-dependent vibration of multi-span micropipes conveying fluid based on modified couple stress theory. J. Phys. Conf. Ser. 1064, 012074.
Zhao, X., Wang, C., Zhu, W., Li, Y., Wan, X., 2021. Coupled thermoelastic nonlocal forced vibration of an axially moving micro/nano-beam. Int. J. Mech. Sci. 206, 106600.
Zhou, W., Chen, W., Muhammad, Lim, C.W., 2019. Surface effect on the propagation of flexural waves in periodic nano-beam and the size-dependent topological properties. Compos. Struct. 216, 427–435.
Zienkiewicz, O., Taylor, R., Zhu, J., 2005. The Finite Element Method: Its Basis and Fundamentals. Elsevier, Science.